

# LaTeXTrans: Structured LaTeX Translation with Multi-Agent Coordination

Ziming Zhu<sup>1\*</sup>, Chenglong Wang<sup>1\*</sup>, Shunjie Xing<sup>1</sup>, Yifu Huo<sup>1</sup>, Fengning Tian<sup>2</sup>,  
Quan Du<sup>2</sup>, Di Yang<sup>1,2</sup>, Chunliang Zhang<sup>1,2</sup>, Tong Xiao<sup>1,2†</sup> and Jingbo Zhu<sup>1,2</sup>

<sup>1</sup> School of Computer Science and Engineering, Northeastern University, Shenyang, China

<sup>2</sup> NiuTrans Research, Shenyang, China

{zhuzm0721, clwang1119}@gmail.com, {xiaotong, zhujingbo}@mail.neu.edu.cn

## Abstract

Despite the remarkable progress of modern machine translation (MT) systems on general-domain texts, translating structured LaTeX-formatted documents remains a significant challenge. These documents typically interleave natural language with domain-specific syntax, such as mathematical equations, tables, figures, and cross-references, all of which must be accurately preserved to maintain semantic integrity and compilability. In this paper, we introduce LaTeXTrans, a collaborative multi-agent system designed to address this challenge. LaTeXTrans ensures format preservation, structural fidelity, and terminology consistency through six specialized agents: 1) a *Parser* that decomposes LaTeX into translation-friendly units via placeholder substitution and syntax filtering; 2) a *Translator*, *Validator*, *Summarizer*, and *Terminology Extractor* that work collaboratively to ensure context-aware, self-correcting, and terminology-consistent translations; 3) a *Generator* that reconstructs the translated content into well-structured LaTeX documents. Experimental results demonstrate that LaTeXTrans can outperform mainstream MT systems in both translation accuracy and structural fidelity, offering an effective and practical solution for translating LaTeX-formatted documents.



System



Video

## 1 Introduction

LaTeX is a widely adopted macro package system built on top of TeX, designed to facilitate the typesetting of complex and structured documents. It has become the de facto standard for scholarly publications across a wide range of scientific disciplines. According to recent statistics, nearly 98% of scientific papers are published in English, while only about 3% of the global population speaks English as their first language (Kleidermacher and

Zou, 2025). This linguistic disparity places considerable pressure on non-native English speakers, who are frequently required to read or write LaTeX-formatted documents in English. As a result, the technical barriers to academic learning and research are significantly increased.

A straightforward approach to ease this burden is to translate LaTeX documents into the user’s native language by processing the compiled PDF version, a process referred to as *PDF translation*. However, this approach often results in incomplete formatting due to errors in PDF parsing. In contrast, a more promising alternative is to translate directly at the LaTeX source level and then compile the translated content into a target-language PDF document. This approach can preserve structural information and allows better control over formatting.

However, translating LaTeX source files presents unique challenges not encountered in plain-text translation. LaTeX documents interleave natural language with domain-specific markup, such as mathematical equations, citation commands, and formatting environments, all of which must be precisely preserved to ensure semantic correctness and successful compilation. Naively applying standard MT systems to LaTeX code typically leads to broken syntax, semantic errors, or formatting loss, ultimately hindering rather than helping the user.

To address these challenges, in this paper, we introduce LaTeXTrans, a collaborative multi-agent system designed to directly translate LaTeX source files while preserving their structural and semantic integrity. Our LaTeXTrans operates on raw LaTeX code and maintains the full syntactic and semantic structure of the document throughout the entire translation pipeline. Specifically, it comprises three modules and six specialized agents:

- *Parsing Module*: Responsible for fine-grained analysis of LaTeX-formatted documents. To handle the structural complexity of LaTeX, we

\* Authors contributed equally.

† Corresponding author.

design a *Parser* agent equipped with a placeholder mechanism and a syntax filter, which together decompose the source into manageable translation units.

- *Translation Module*: This module leverages a team of collaborative agents, including a *Translator*, *Validator*, *Summarizer*, and *Terminology Extractor*, which work together to perform context-aware and self-correcting translation of the parsed units.
- *Generation Module*: A *Generator* agent reconstructs the translated document by reinserting the translated content into the original LaTeX structure, producing well-formatted LaTeX source in the target language.

To evaluate the effectiveness of LaTeXTrans, we first construct a LaTeX source test set using TeX files collected from arXiv papers. We then compare LaTeXTrans with a range of MT and LLM-based translation baselines. Experimental results demonstrate that LaTeXTrans consistently outperforms all baselines in both translation accuracy and format fidelity. Notably, LaTeXTrans achieves an improvement of 13.20 points on FC-score, along with significant gains in COMETkiwi and LLM-score when compared to GPT-4o.

## 2 Related works

**LLM-based Machine Translation.** The emergence of LLMs has introduced a new paradigm for MT, shifting away from traditional supervised learning on parallel corpora toward more flexible, general-purpose language understanding (Gain et al., 2025). LLMs like GPT-3 (Brown et al., 2020), PaLM (Chowdhery et al., 2022), and GPT-4 demonstrate strong multilingual capabilities without explicit training on translation tasks. LLM-based translation leverages in-context learning, where the model is prompted with examples or instructions to perform translation on the fly. This approach has shown competitive performance in zero-shot and few-shot learning scenarios (Vilar et al., 2023), especially for high-resource language pairs. Unlike traditional neural machine translation (NMT), which requires retraining or fine-tuning for each new domain or language, LLMs can generalize across tasks and languages with minimal additional data.

**Multi-Agent Systems.** More recently, the emergence of LLMs has opened new possibilities for Multi-Agent Systems (MAS). In LLM-based multi-agent systems, each agent is instantiated as an LLM-powered entity capable of natural language reasoning, planning, and collaboration. Systems such as AutoGPT (Yang et al., 2023), CAMEL (Li et al., 2023), and AutoGen (Dibia et al., 2024) demonstrate that LLM agents can simulate diverse roles and complete complex tasks through dialogue-based coordination. A growing number of studies explore the use of multi-agent systems for translation-related tasks. Notably, MAS has emerged as a promising solution for document-level translation (Wang et al., 2024), a long-standing challenge in MT.

**Formatted Text Translation.** Formatted text translation involves translating documents that contain structural or semantic markup, such as LaTeX and XML. These formats often interleave natural language with commands, tags, or tokens that encode formatting, layout, or semantic annotations. Although some recent efforts have been made in this direction (Kleidermacher and Zou, 2025; Khan, 2025), formatted text translation still faces two major challenges. The first is the lack of a robust, general-purpose system specifically designed for translating formatted content. Currently, only a few proprietary tools, such as Youdao and Baidu, offer relatively effective solutions. While open-source tools like MathTranslate\* and GPT-Academic† have received positive feedback, they still lag behind commercial systems in overall performance. The second is the lack of a sound, formatted text translation evaluation technique. As traditional BLEU or COMET scores do not cover format correctness or tag retention. Therefore, it is imperative to develop a new evaluation technique for structure-aware translation.

## 3 System Design

The key architecture of LaTeXTrans is a multi-agent coordination designed for translating structured LaTeX documents. It consists of three modules: the Parser, the Translation Module, and the Generation Module. The design and functionality of each component are described in detail below.

\*<https://github.com/SUSYUSTC/MathTranslate>

†[https://github.com/binary-husky/gpt\\_academic](https://github.com/binary-husky/gpt_academic)

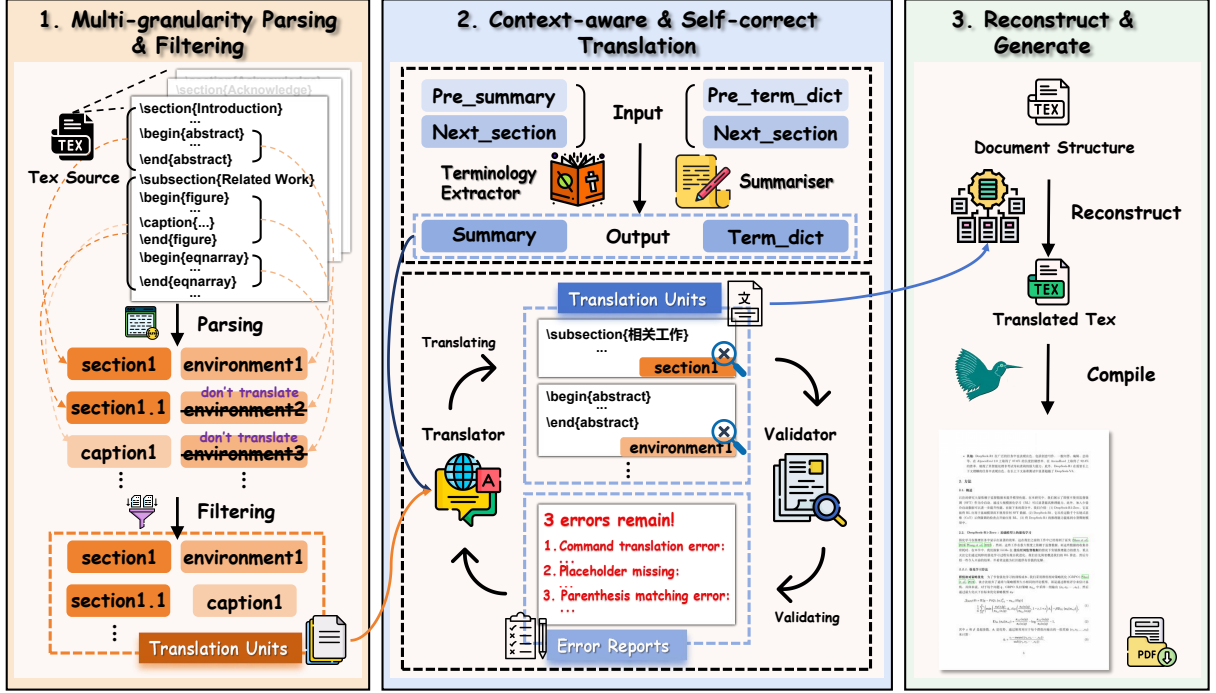


Figure 1: The architecture of our LaTeXTrans system.

### 3.1 Parser Module

Structured LaTeX documents interleave natural language content with formatting commands and semantic markup, resulting in tightly coupled representations that are not well-suited for direct translation by LLMs. Naively feeding the entire document to an LLM leads to several issues: unnecessary processing of non-translatable components, increased computational cost, and a higher risk of introducing translation errors. To address these challenges, we introduce the Parser module, which serves as the first stage of the LaTeXTrans pipeline. Its basic idea is to transform complex LaTeX documents into clean, structured translation units that are easier for LLMs to process. Specifically, we design a placeholder substitution strategy to temporarily replace LaTeX-specific commands and environments, and implement a filtering mechanism to remove components that do not require translation.

**Placeholder Substitution Strategy.** For a common LaTeX document, our placeholder substitution strategy is shown in Figure 2. We consider that the original mathematical formulas and charts are retained during translation. The first step is to replace the captions in the chart with placeholders. The second step is to replace the environment with placeholders, which will include the vast majority of mathematical formulas, charts, and other parts that do not need to be translated. Finally, we split

the replaced text into sections (including subsections and subsubsections). For a LaTeX project composed of multiple tex files, we first merge the necessary tex files into the main file and then insert placeholders at the beginning and end of the merge for future restoration. The subsequent placeholder replacement rules and segmentation methods are the same as before. From the placeholder substitution strategy, we obtain translation units of two granularities: context (i.e., section and environment) and sentence (i.e., caption).

**Translation Unit Filter.** While non-translatable components are replaced with placeholders, we notice that LaTeX allows users to define custom environments, making it infeasible to rely solely on exhaustive rule-based approaches to identify all such segments. To address this issue, we complement a predefined list of protected environments with a Filter agent powered by an LLM, which dynamically determines whether a given environment requires translation. Each extracted environment is annotated with a binary label: True or False. The translation module subsequently processes only those segments labeled as True.

### 3.2 Translation Module

The translation module comprises four agents: the Translator, Validator, Summarizer, and Terminology Extractor. After the Translator completes the

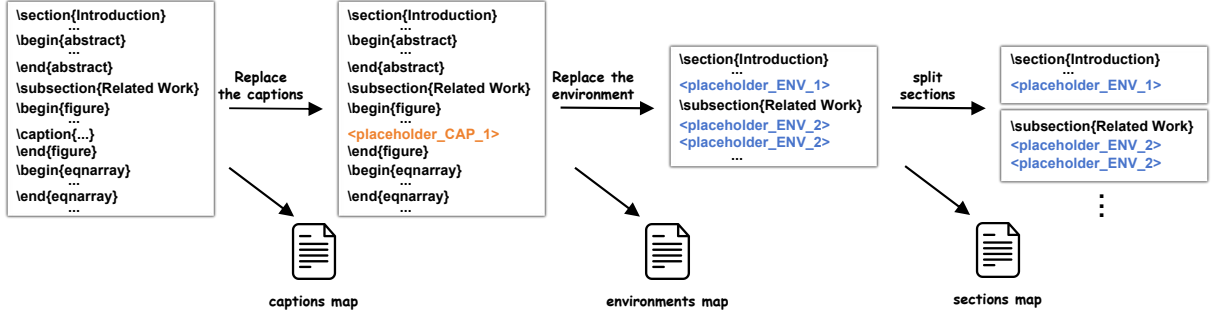


Figure 2: The pipeline of our placeholder substitution strategy. The mapping files are the mapping of placeholders and the replaced content, and they are also translation units of different granularities.

translation of all designated units, the output is passed to the Validator, which generates an error report and returns it for revision if necessary. The Summarizer and Terminology Extractor assist the Translator by providing a summary of the preceding content and a domain-specific terminology dictionary, respectively, thereby enhancing contextual coherence and ensuring terminology consistency throughout the translation process.

**Translator-Validator Iteration.** When utilizing large-context windows for document translation, large language models (LLMs) often prioritize capturing the overall meaning of the text, which can result in the omission or mistranslation of individual sentences (Wang et al., 2024). This issue is particularly pronounced in LaTeX document translation, where LLMs may neglect or incorrectly render LaTeX commands. For example, the command “`\textbf{}`” may be omitted, or “`\left`” may be incorrectly translated as “`\左`”. Due to the structured and sensitive syntax of LaTeX, such errors are frequent and can lead to compilation failures. To address this issue, we introduce a Translator-Validator iterative framework, which performs multiple rounds of verification to progressively improve LaTeX command preservation for each translation unit. This iterative refinement significantly enhances the usability and reliability of the overall translation system. Specifically, as illustrated in Figure 1, after the Translator has completed the translation of all translation units, the Validator will verify the quality of the translation from three dimensions and eventually generate an error report. When conducting the next round of translation, the erroneous translation units, together with the error reports, will form the prompt for the Translator to guide them in generating the correct translation.

**Summarizer and Terminology Extractor.** Inspired by Wang et al. (2024)’s work, we design a

Summarizer and Terminology Extractor to enhance the contextual coherence and terminology consistency of translation. Specifically, the Summarizer is responsible for constantly generating and updating the summary of the previous text during the translation process. When each translation unit is completed, the Summarizer will combine the previous summary with the original text of the current translation unit to generate a new summary. The Terminology Extractor is responsible for maintaining a terminology dictionary and adding it to the prompt of the Translator to provide a reference for terminology translation for the Translator. When the Translator finishes the translation of a translation unit, the Terminology Extractor extracts term pairs from the original text and the translation and updates the term dictionary in real-time.

### 3.3 Generation Module

The generation module is responsible for reassembling the translation units into structured LaTeX documents and compiling the structured LaTeX documents into PDF files using specific compilers (e.g. pdfL<sup>A</sup>T<sub>E</sub>X and XeL<sup>A</sup>T<sub>E</sub>X).

## 4 Experiment

### 4.1 Settings

**Datasets.** Since no publicly available LaTeX document dataset currently exists, we constructed our test set by selecting the TeX sources of 50 English academic papers from the arXiv repository. The chosen papers include both long and short articles, many of which contain complex formulas and figures, ensuring structural diversity and complexity in the LaTeX content. Further experimental details are provided in Appendix A.

**Baselines.** Our baselines are categorized into two groups: traditional MT systems and LLM-based



System	En-Zh				En-Ja			
	Cometkiwi (↑)	LLM-score (↑)	FC-score (↑)	Cost (↓)	Cometkiwi (↑)	LLM-score (↑)	FC-score (↑)	Cost (↓)
NiuTrans	64.69	7.93	60.72	-	65.49	8.19	27.48	-
Google Translate	46.23	5.93	51.00	-	56.21	7.01	50.00	-
LLaMA-3.1-8b	42.89	2.92	49.40	-	44.49	3.32	60.92	-
Qwen-3-8b	45.55	7.87	48.68	-	46.20	6.80	49.52	-
Qwen-3-14b	68.18	8.76	65.63	-	72.84	8.66	61.88	-
DeepSeek-V3	67.26	<b>9.02</b>	63.68	<b>\$0.02</b>	72.17	<b>9.00</b>	63.96	<b>\$0.03</b>
GPT-4o	67.22	8.58	58.32	\$0.13	71.16	8.91	56.92	\$0.11
LaTeXTrans <sub>Qwen-3-14b</sub>	71.37	8.97	71.20	-	74.68	8.51	59.84	-
LaTeXTrans <sub>DeepSeek-V3</sub>	73.48	9.01	70.52	\$0.10	<b>75.39</b>	8.89	<b>66.52</b>	\$0.13
LaTeXTrans <sub>GPT-4o</sub>	<b>73.59</b>	8.92	<b>71.52</b>	\$0.35	74.47	8.93	64.92	\$0.45

Table 1: COMETkiwi, FC-score, and LLM-score comparisons across different systems. We also report the cost incurred when using the official API to translate each paper on average in the test set, as shown in the “Cost” column. **Bold** indicates the best result in each group.

translation systems. For the former, we selected NiuTrans and Google Translate as representative systems. For the latter, we evaluated five strong LLMs, including both open-source and proprietary models: LLaMA-3.1-8B (Grattafiori et al., 2024), Qwen-3-8B (Yang et al., 2025), Qwen-3-14B, DeepSeek-V3 (Liu et al., 2024), and GPT-4o (Hurst et al., 2024). Among these, Qwen-3-14B, DeepSeek-V3, and GPT-4o were further used as the backbone models for agents in LaTeXTrans.

## 4.2 Evaluation Metrics

We conducted a comprehensive assessment of our system from two dimensions: translation quality and format retention ability.

**Translation Quality.** Because high-quality reference translations for LaTeX documents require expert-level annotation, we adopted wmt22-cometkiwi-da (Rei et al., 2022), a reference-free evaluation metric (denoted as *Cometkiwi*), to assess the translation quality of LaTeX documents. Furthermore, we employed GPT-4o as an automatic evaluator to further assess translation quality across multiple dimensions, guided by carefully designed system prompts. The evaluation covered four aspects: Faithfulness, Fluency, Terminology Consistency, and Coherence, where each was rated on a scale from 0 to 10. An overall score was then synthesized by GPT-4o based on the individual scores across these dimensions (denoted as *LLM-score*).

**Format Retention Ability.** Whether the labels are completely retained is an important manifestation of the ability of the formatted text translation system. However, at present, there is no universal indicator to evaluate the format retention ability of models or systems during the translation process. Therefore, for LaTeX documents, we have designed a new evaluation metric, **Format**

**Consistency Score** (denoted as *FC-score*), to assess the retention ability of our system for LaTeX labels during the translation process. We can compute the FC-score by

$$\text{FC-score} = S_0 - \alpha N_e - \beta N_w + \gamma C \quad (1)$$

where  $S_0$  is the initial score before the rewards and penalties,  $\alpha$  is the penalty coefficient per error,  $\beta$  is the penalty coefficient per warning,  $\gamma$  is the reward for successful compilation.  $N_e$  and  $N_w$  are numbers of errors and warnings,  $C \in \{0, 1\}$  indicates whether the LaTeX document compiled successfully. We then clip the score to the valid range  $[S_{\min}, S_{\max}]$ ,  $S_{\max}$  and  $S_{\min}$  are the upper bound and lower bound of the score (e.g. 0~100).

## 4.3 Results

We evaluate our LaTeXTrans system on two translation tasks: English-to-Chinese (En-Zh) and English-to-Japanese (En-Ja). The results, shown in Table 1, demonstrate that LaTeXTrans consistently outperforms both the NMT and Single-Agent baselines across all evaluation metrics, including COMETkiwi and FC-score. In terms of translation quality, LaTeXTrans demonstrates substantial improvements in FC-score (71.52 vs. 58.32 for the En-Zh task and 70.52 vs. 63.68 for the En-Ja task), indicating significantly better preservation of LaTeX formatting during translation. Moreover, when powered by GPT-4o as the backbone model, LaTeXTrans achieves the highest scores across all three evaluation metrics—COMETkiwi, LLM-score, and FC-score—underscoring its strong overall translation performance on structured LaTeX documents. In terms of translation cost, LaTeXTrans delivers superior performance without incurring a substantial increase in computational expense compared to other LLM-based translation

Tex source 1	Tex source 2
<pre> \paragraph{Self-Attention} Each token yields a \emph{query}, \emph{key}, and \emph{value}: \[\mathbf{q} = \mathbf{xW}^Q, \mathbf{k} = \mathbf{xW}^K\] This enables computing attention weights via token similarity. ... \paragraph{Contextual Encoding} Based on the query-key similarity in the previous section, we compute: \[\text{Attention} = \text{softmax}\left(\frac{\mathbf{q}\mathbf{k}^T}{\sqrt{d_k}}\right)\mathbf{v}\] The same projections are reused across layers. </pre>	<pre> \section{Transformers blocks need to avoid over-mixing} \label{sec:theory} We present mathematical insights that aim to understand why the \emph{formation of attention sinks} can be useful or even \emph{necessary} ... \begin{theorem}[More detailed over-squashing bounds.] Let <math>C_{\max} &gt; 0</math> be the greatest Lipschitz constant of any layer of the Transformer, <math>H</math> be the number of heads, and <math>\delta_i</math> be <math>1</math> iff <math>i=j</math> and <math>0</math> otherwise. </pre>
Baseline	
<pre> \paragraph{自注意力} 每个token都会生成一个\emph{查询}、\emph{键}和\emph{值}： \[\mathbf{q} = \mathbf{xW}^Q, \mathbf{k} = \mathbf{xW}^K\] 这让我们可以通过token间的相似度来计算注意力权重。 ... \paragraph{上下文编码} 根据前一节中的query-key相似度，我们计算： \[\text{注意力} = \text{softmax}\left(\frac{\mathbf{q}\mathbf{k}^T}{\sqrt{d_k}}\right)\mathbf{v}\] 相同的投影矩阵在不同层之间被复用。 </pre>	<pre> \section{Transformer模块需要避免过度混合} \label{sec:theory} 我们提出数学见解，旨在理解？注意力汇集的形成为何有用甚至\emph{必要}。 ... \begin{theorem}[更详细的过度压缩界限。] 设 <math>C_{\max} &gt; 0</math> 为Transformer任一层的 最大李普希茨常数，<math>H</math> 为头数，<math>\delta_i</math> 为 <math>1</math> 当且仅当 <math>i=j</math>，否则为 <math>0</math>。 </pre>
LaTeXTrans	
<pre> \paragraph{自注意力} 每个token都会生成一个\emph{query}、\emph{key}和\emph{value}： \[\mathbf{q} = \mathbf{xW}^Q, \mathbf{k} = \mathbf{xW}^K\] 这让我们可以通过token间的相似度来计算注意力权重。 ... \paragraph{上下文编码} 基于上一节中query-key相似度，我们定义注意力机制如下： \[\text{Attention} = \text{softmax}\left(\frac{\mathbf{q}\mathbf{k}^T}{\sqrt{d_k}}\right)\mathbf{v}\] 所有网络层共享相同的投影矩阵。 </pre>	<pre> \section{Transformer块需要避免过度混合} \label{sec:theory} 我们提出了数学见解，旨在理解为什么\emph{注意力汇集的形成}可能是有用的甚至 是\emph{必要的}。 ... \begin{theorem}[更详细的过度压缩界限。] 设 <math>C_{\max} &gt; 0</math> 是Transformer中 任意一层的最大Lipschitz常数，<math>H</math>是头的数量，且<math>\delta_i</math>在<math>i=j</math>时为 <math>1</math>，否则为<math>0</math>。 </pre>

Figure 3: Comparison of translation quality in two representative cases between the baseline and LaTeXTrans. In the LaTeX source, blue text marks labels that should be preserved. A red question mark (“?”) indicates label loss during translation. Red highlights inconsistent translations, green indicates consistent ones, and orange shows LaTeX labels missed by the baseline but successfully preserved by LaTeXTrans.

systems, making it well-suited for large-scale deployment in real-world applications.

#### 4.4 Ablation Study

Table 2 presents an ablation study on the En-Zh task using GPT-4o and DeepSeek-V3 as backbone models. Introducing the Parser module significantly improves both COMETkiwi and FC-score, indicating that the placeholder substitution strategy enhances translation quality and label preservation. Adding the Validator module further boosts overall performance, although a slight drop in LLM-score is observed with DeepSeek-V3. We hypothesize that this is due to the Validator enforcing strict tag retention through iterative checks, which may restrict the Translator and slightly impact fluency. Finally, incorporating the Summarizer and Terminology Extractor improves the LLM-score, reflecting better cross-paragraph coherence. However, slight declines in COMETkiwi and FC-score suggest that these improvements may not be fully captured by COMETkiwi. A detailed analysis with a case study is provided in Section 4.4.1.

##### 4.4.1 Translation consistency

We present a case study of the En-Zh task from our test set to demonstrate that our system does indeed perform better in terms of translation con-

Setting	GPT-4o			DeepSeek-V3		
	Cometkiwi	LLM-score	FC-score	Cometkiwi	LLM-score	FC-score
SA. (Baseline)	67.22	8.58	58.32	67.26	9.02	63.68
SA. + P.	74.47	8.89	69.64	74.39	9.03	70.08
SA. + P. + V.	<b>74.57</b>	8.91	<b>71.76</b>	<b>74.42</b>	8.94	<b>70.80</b>
SA. + P. + V. + S.	74.06	<b>8.95</b>	71.64	74.02	<b>9.05</b>	70.68
SA. + P. + V. + S. + TE.	73.59	8.93	71.52	73.48	9.01	70.52

Table 2: Performance of LaTeXTrans with different settings. “SA.” denotes the LLM-based translation baseline, “P.” stands for the Parser, “V.” for the Validator, “S.” for summarizer, and “TE.” for the Terminology Extractor. The “SA. + P. + V. + S. + TE.” corresponds to our LaTeXTrans.

sistency, as shown in Figure 3. In this case, the terminology translation of LaTeXTrans remains consistent across the three sections. In contrast, the baseline method finds it difficult to maintain such consistency. This indicates that our system can maintain excellent consistency throughout the entire translation process.

## 5 Conclusion

In this paper, we propose LaTeXTrans, a multi-agent system for translating structured LaTeX documents. LaTeXTrans consists of three collaborative modules, each responsible for a specific stage of the translation pipeline. Experimental results demonstrate that LaTeXTrans can outperform baseline systems and offer a reliable solution for LaTeX document translation.

## Limitations

Any instruction-following LLM can be integrated into our LaTeXTrans system. However, due to the large number of available models, it is impractical to evaluate each one individually. Therefore, we select a representative subset of commonly used LLMs for our experiments. We believe this selection sufficiently demonstrates the practicality and effectiveness of LaTeXTrans for LaTeX document translation. Additionally, although commercial systems such as Baidu and Youdao offer LaTeX translation services, they are not open-source. As a result, we are unable to compute metrics like COMETkiwi and FC-score for these systems. Therefore, we do not include a comprehensive comparison with them in our main experiments.

## References

- Tom B. Brown, Benjamin Mann, Nick Ryder, Melanie Subbiah, Jared Kaplan, Prafulla Dhariwal, Arvind Neelakantan, Pranav Shyam, Girish Sastry, Amanda Askell, Sandhini Agarwal, Ariel Herbert-Voss, Gretchen Krueger, Tom Henighan, Rewon Child, Aditya Ramesh, Daniel M. Ziegler, Jeffrey Wu, Clemens Winter, and 12 others. 2020. [Language models are few-shot learners](#). In *Advances in Neural Information Processing Systems 33: Annual Conference on Neural Information Processing Systems 2020, NeurIPS 2020, December 6-12, 2020, virtual*.
- Aakanksha Chowdhery, Sharan Narang, Jacob Devlin, Maarten Bosma, Gaurav Mishra, Adam Roberts, Paul Barham, Hyung Won Chung, Charles Sutton, Sebastian Gehrmann, Parker Schuh, Kensen Shi, Sasha Tsvyashchenko, Joshua Maynez, Abhishek Rao, Parker Barnes, Yi Tay, Noam Shazeer, Vinodkumar Prabhakaran, and 48 others. 2022. [Palm: Scaling language modeling with pathways](#).
- Victor Dibia, Jingya Chen, Gagan Bansal, Suff Syed, Adam Fourney, Erkang Zhu, Chi Wang, and Saleema Amershi. 2024. [Autogen studio: A no-code developer tool for building and debugging multi-agent systems](#).
- Baban Gain, Dibyanayan Bandyopadhyay, and Asif Eklal. 2025. [Bridging the linguistic divide: A survey on leveraging large language models for machine translation](#).
- Aaron Grattafiori, Abhimanyu Dubey, Abhinav Jauhri, Abhinav Pandey, Abhishek Kadian, Ahmad Al-Dahle, Aiesha Letman, Akhil Mathur, Alan Schelten, Alex Vaughan, and 1 others. 2024. [The llama 3 herd of models](#). *ArXiv preprint*, abs/2407.21783.
- Aaron Hurst, Adam Lerer, Adam P Goucher, Adam Perelman, Aditya Ramesh, Aidan Clark, AJ Ostrow, Akila Welihinda, Alan Hayes, Alec Radford, and 1 others. 2024. [Gpt-4o system card](#). *ArXiv preprint*, abs/2410.21276.
- Ishup Ali Khan. 2025. Xml and json translator. Master’s thesis, master of business administration, ict services and systems, Haaga-Helia University of Applied Sciences. Permanent link: [urlhttps://urn.fi/URN:NBN:fi:amk-2025060521005](https://urn.fi/URN:NBN:fi:amk-2025060521005).
- Hannah Calzi Kleidermacher and James Zou. 2025. [Science across languages: Assessing llm multilingual translation of scientific papers](#).
- Guohao Li, Hasan Hammoud, Hani Itani, Dmitrii Khizbullin, and Bernard Ghanem. 2023. [CAMEL: communicative agents for "mind" exploration of large language model society](#). In *Advances in Neural Information Processing Systems 36: Annual Conference on Neural Information Processing Systems 2023, NeurIPS 2023, New Orleans, LA, USA, December 10 - 16, 2023*.
- Aixin Liu, Bei Feng, Bing Xue, Bingxuan Wang, Bochao Wu, Chengda Lu, Chenggang Zhao, Chengqi Deng, Chenyu Zhang, Chong Ruan, and 1 others. 2024. [Deepseek-v3 technical report](#). *ArXiv preprint*, abs/2412.19437.
- Ricardo Rei, Marcos Treviso, Nuno M. Guerreiro, Chrysoula Zerva, Ana C Farinha, Christine Maroti, José G. C. de Souza, Taisiya Glushkova, Duarte Alves, Luisa Coheur, Alon Lavie, and André F. T. Martins. 2022. [CometKiwi: IST-unbabel 2022 submission for the quality estimation shared task](#). In *Proceedings of the Seventh Conference on Machine Translation (WMT)*, pages 634–645, Abu Dhabi, United Arab Emirates (Hybrid). Association for Computational Linguistics.
- David Vilar, Markus Freitag, Colin Cherry, Jiaming Luo, Viresh Ratnakar, and George Foster. 2023. [Prompting PaLM for translation: Assessing strategies and performance](#). In *Proceedings of the 61st Annual Meeting of the Association for Computational Linguistics (Volume 1: Long Papers)*, pages 15406–15427, Toronto, Canada. Association for Computational Linguistics.
- Yutong Wang, Jiali Zeng, Xuebo Liu, Derek F. Wong, Fandong Meng, Jie Zhou, and Min Zhang. 2024. [Delta: An online document-level translation agent based on multi-level memory](#).
- An Yang, Anfeng Li, Baosong Yang, Beichen Zhang, Binyuan Hui, Bo Zheng, Bowen Yu, Chang Gao, Chengen Huang, Chenxu Lv, and 1 others. 2025. [Qwen3 technical report](#). *ArXiv preprint*, abs/2505.09388.
- Hui Yang, Sifu Yue, and Yunzhong He. 2023. [Autogpt for online decision making: Benchmarks and additional opinions](#).

## A Additional Detailed Settings of the Experiment

**Baselines.** Since the dataset consisted entirely of structured LaTeX documents which exceeded the handling capabilities of single-model systems, we adopted a preprocessing step in the baseline approach. Specifically, the structured LaTeX documents were segmented into section-level translation units to make them manageable for translation.

**Hyperparameter Setting.** In the experiments, we evaluated both open-source and closed-source models separately. For the closed-source models, we accessed them via a third-party API. In the baseline approach, we set the maximum number of new tokens to 16,384 and the temperature to 0.7, while keeping all other hyperparameters at their default values. For our system, the temperature in the Filter was set to 0 with a maximum of 50 new tokens, while all other agents were configured with a maximum of 8,192 new tokens; the remaining hyperparameters were kept at their defaults.

**Evaluation.** When computing COMETkiwi and LLM-scores, we used `pylatexenc`<sup>‡</sup> to convert each LaTeX translation unit into plain text. Although LaTeXTrans parses structured LaTeX documents into fine-grained translation units, we followed the baseline’s evaluation protocol by using section-level translation units for computing both COMETkiwi and LLM-scores. Furthermore, to assess contextual consistency in the LLM-score evaluation, we concatenated section-level translation units into paired paragraphs and then scored them using GPT-4o. The prompt template used for scoring is illustrated in Figure 12. When calculating the FC-score, we set the initial score  $S_0$  to 100. Since errors have a greater impact on the final PDF format scheduling effect than warnings, in the experiment, we set the value of  $\alpha$  (10) to be significantly greater than  $\beta$  (2). Ultimately, whether the compilation is successful is the most intuitive factor for evaluating the compilation. Therefore, in the experiment, we set the  $\gamma$  to 20.

**Datasets** We selected the LaTeX source files of 50 academic papers in the field of computer science from arXiv as our test set. The distribution of paper lengths is shown in Figure 4. Additionally, we analyzed the topics of the papers and visualized them as a word cloud in Figure 5. This result shows

that the test set exhibits a diverse range of paper lengths, covering both short and long documents, which helps ensure robustness across different document sizes. Moreover, the word cloud reveals a wide variety of research topics within the computer science domain, confirming the topical diversity of the test set and enhancing the generality of our evaluation.

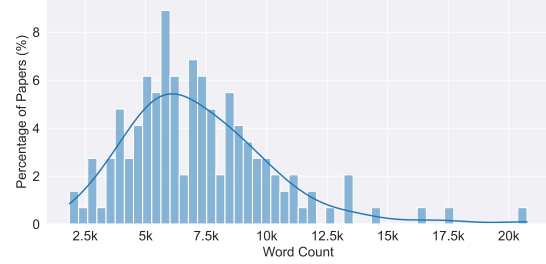


Figure 4: Distribution of paper lengths (in word count) in our test set.

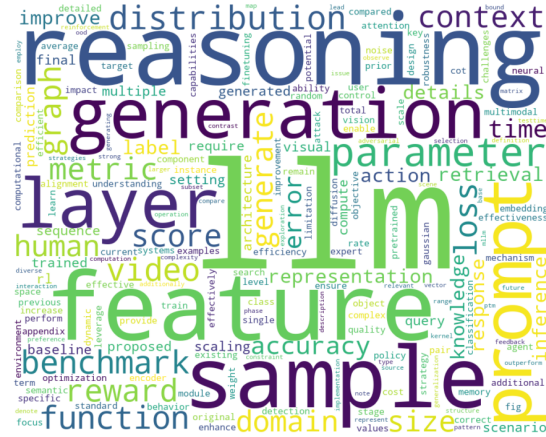


Figure 5: Word cloud visualization of topics covered in our test set.

## B System Performance Display

We select six cases to visually demonstrate the translation performance of our system, focusing on En-Zh and En-Ja translation tasks, as illustrated in Figure 6 to Figure 11. All six cases are translation cases of the LaTeX source code of papers by LaTeXTrans. In each case, we have selected two relatively complex parts to present. Among the six cases, there are three En-Zh translation tasks and three En-Ja translation tasks, respectively.

## C Prompt Templates for LLM-Based Components in LaTeXTrans

Figures 13 through 17 show the prompt templates used by the agents within the LaTeXTrans system.

<sup>‡</sup><https://github.com/phfaist/pylatexenc>



3. We systematically integrate techniques from prior work, such as Clip-Higher and Token-level Loss from DAPO [29], Value-Petraining and Decoupled-GAE from VC-PPO [30], self-imitation learning from SIL [14], and Group-Sampling from GRPO [22]. Additionally, we further validate their necessity through ablation studies.

**VAPO** is an effective reinforcement learning system that brings together these improvements. These enhancements work together smoothly, leading to a combined result that's better than the sum of the individual parts. We conduct experiments using the Qwen2.5-32B pre-trained model, ensuring no SFT data is introduced in any of the experiments, to maintain comparability with related works (DAPO and DeepSeek-RL-Zero-Qwen-32B). The performance of **VAPO** improves from vanilla PPO a score of 5 to 60, surpassing the previous SOTA value-model-free methods DAPO [29] by 10 points. More importantly, **VAPO** is highly stable — we don't observe any crashes during training, and the results across multiple runs are consistently similar.

## 2 Preliminaries

This section presents the fundamental concepts and notations that serve as the basis for our proposed algorithm. We first explore the basic framework of representing language generation as a reinforcement learning task. Subsequently, we introduce Proximal Policy Optimization and Generalized Advantage Estimation.

### 2.1 Modeling Language Generation as Token-Level MDP

Reinforcement learning centers around the learning of a policy that maximizes the cumulative reward for an agent as it interacts with an environment. In this study, we cast language generation tasks within the framework of a Markov Decision Process (MDP) [17].

Let the prompt be denoted as  $x$ , and the response to this prompt as  $y$ . Both  $x$  and  $y$  can be decomposed into sequences of tokens. For example, the prompt  $x$  can be expressed as  $x = (x_0, \dots, x_m)$ , where the tokens are drawn from a fixed discrete vocabulary  $\mathcal{A}$ .

We define the token-level MDP as the tuple  $\mathcal{M} = (\mathcal{S}, \mathcal{A}, \mathbb{P}, R, d_0, \omega)$ . Here is a detailed breakdown of each component:

- **State Space (S):** This space encompasses all possible states formed by the tokens generated up to a given time step  $t$ . At time step  $t$ , the state  $s_t$  is defined as  $s_t = (x_0, \dots, x_m, y_0, \dots, y_t)$ .
- **Action Space (A):** It corresponds to the fixed discrete vocabulary, from which tokens are selected during the generation process.
- **Dynamics (P):** These represent a deterministic transition model between tokens. Given a state  $s_t = (x_0, \dots, x_m, y_0, \dots, y_t)$ , an action  $a = y_{t+1}$ , and the subsequent state  $s_{t+1} = (x_0, \dots, x_m, y_0, \dots, y_t, y_{t+1})$ , the probability  $\mathbb{P}(s_{t+1}|s_t, a) = 1$ .
- **Termination Condition:** The language generation process concludes when the terminal action  $\omega$ , typically the end-of-sentence token, is executed.
- **Reward Function  $R(s_t, a)$ :** This function offers scalar feedback to evaluate the agent's performance after taking action  $a$  in state  $s_t$ . In the context of Reinforcement Learning from Human Feedback (RLHF) [18, 23], the reward function can be learned from human preferences or defined by a set of rules specific to the task.
- **Initial State Distribution  $d_0$ :** It is a probability distribution over prompts  $x$ . An initial state  $s_0$  consists of the tokens within the prompt  $x$ .

### 2.2 RLHF Learning Objective

We formulate the optimization problem as a KL-regularized RL task. Our objective is to approximate the optimal KL-regularized policy, which is given by:

$$\pi^* = \arg \max_{\pi} \mathbb{E}_{s_0 \sim d_0} \left[ \sum_{t=0}^H (R(s_t, a_t) - \beta \text{KL}(\pi(\cdot|s_t) \parallel \pi_{\text{ref}}(\cdot|s_t))) \right] \quad (1)$$

3

(a) The first part of the English PDF of case 1.

GRPO [22] 的组采样。此外，我们通过消融研究进一步验证了它们的必要性。

**VAPO** 是一个有效的强化学习系统，将这些改进结合在一起。这些增强措施协同工作，导致合并结果优于各个部分的简单相加。我们使用Qwen2.5-32B预训练模型进行实验，确保在任何实验中都没有引入SFT数据，以保持与相关工作的可比性（DAPO 和 DeepSeek-RL-Zero-Qwen-32B）。**VAPO** 的性能从原始PPO的得分5提高到60，超过了之前的SOTA无价值模型方法DAPO [29] 10分。更重要的是，**VAPO** 高度稳定——我们在训练期间没有观察到任何崩溃，并且多次运行的结果始终相似。

## 2 预备知识

本节介绍作为我们所提算法基础的基本概念和符号。我们首先探讨将语言生成表示为强化学习任务的基本框架。随后，我们介绍近端策略优化和广义优势估计。

### 2.1 将语言生成建模为令牌级MDP

强化学习的核心是学习一种策略，使代理在与环境交互时最大化累积奖励。在本研究中，我们将语言生成任务置于马尔可夫决策过程（MDP）的框架内 [17]。

令提示表示为  $x$ ，对该提示的响应表示为  $y$ 。  $x$  和  $y$  都可以分解为令牌序列。例如，提示  $x$  可以表示为  $x = (x_0, \dots, x_m)$ ，其中令牌来自固定的离散词汇  $\mathcal{A}$ 。

我们将令牌级MDP定义为元组  $\mathcal{M} = (\mathcal{S}, \mathcal{A}, \mathbb{P}, R, d_0, \omega)$ ，以下是每个组件的详细信息：

- **状态空间 (S):** 此空间包含了在给定时间步之前生成的所有可能状态。在时间步  $t$ ，状态  $s_t$  定义为  $s_t = (x_0, \dots, x_m, y_0, \dots, y_t)$ 。
- **动作空间 (A):** 它对应于固定的离散词汇表，从中选择生成过程中的标记。
- **动态模型 (P):** 这些表示标记之间的确定性转换模型。给定状态  $s_t = (x_0, \dots, x_m, y_0, \dots, y_t)$ ，动作  $a = y_{t+1}$ ，以及后续状态  $s_{t+1} = (x_0, \dots, x_m, y_0, \dots, y_t, y_{t+1})$ ，则概率  $\mathbb{P}(s_{t+1}|s_t, a) = 1$ 。
- **终止条件:** 语言生成过程在终止动作  $\omega$  执行时结束，通常是句子结束标记。
- **奖励函数  $R(s_t, a)$ :** 此函数提供标量反馈，以评估智能体在状态  $s_t$  下执行动作  $a$  后的表现。在从人类反馈中进行强化学习（RLHF）[18, 23] 的背景下，奖励函数可以从人类偏好中学习，或通过特定任务的规则来定义。
- **初始状态分布  $d_0$ :** 这是一个关于提示  $x$  的概率分布。初始状态  $s_0$  包含提示  $x$  内的标记。

### 2.2 RLHF 学习目标

我们将优化问题表述为一个 KL 正则化的 RL 任务。我们的目标是逼近最优的 KL 正则化策略，其表示为：

$$\pi^* = \arg \max_{\pi} \mathbb{E}_{s_0 \sim d_0} \left[ \sum_{t=0}^H (R(s_t, a_t) - \beta \text{KL}(\pi(\cdot|s_t) \parallel \pi_{\text{ref}}(\cdot|s_t))) \right] \quad (1)$$

3

(b) The first part of the Chinese PDF of case 1.

In this equation,  $H$  represents the total number of decision steps,  $s_0$  is a prompt sampled from the dataset,  $R(s_t, a_t)$  is the token-level reward obtained from the reward function,  $\beta$  is a coefficient that controls the strength of the KL-regularization, and  $\pi_{\text{ref}}$  is the initialization policy.

In traditional RLHF and most tasks related to LLMs, the reward is sparse and is only assigned at the terminal action  $\omega$ , that is, the end-of-sentence token <eos>.

### 2.3 Proximal Policy Optimization

PPO [21] uses a clipped surrogate objective to update the policy. The key idea is to limit the change in the policy during each update step, preventing large policy updates that could lead to instability. Let  $\pi_{\text{old}}(a|s)$  be the policy parameterized by  $\theta$ , and  $\pi_{\text{old}}(a|s)$  be the old policy from the previous iteration. The surrogate objective function for PPO is defined as:

$$\mathcal{L}^{\text{CLIP}}(\theta) = \mathbb{E}_s \left[ \min \left( r_t(\theta) \hat{A}_t, \text{clip}(r_t(\theta), 1 - \epsilon, 1 + \epsilon) \hat{A}_t \right) \right] \quad (2)$$

where  $r_t(\theta) = \frac{\pi_{\text{old}}(a_t|s_t)}{\pi_{\text{old}}(a_t|s_t)}$  is the probability ratio,  $\hat{A}_t$  is the estimated advantage at time step  $t$ , and  $\epsilon$  is a hyperparameter that controls the clipping range.

Generalized Advantage Estimation [20] is a technique used to estimate the advantage function more accurately in PPO. It combines multiple-step bootstrapping to reduce the variance of the advantage estimates. For a trajectory of length  $T$ , the advantage estimate  $\hat{A}_t$  at time step  $t$  is computed as:

$$\hat{A}_t = \sum_{l=0}^{T-t-1} (\gamma \lambda)^l \delta_{t+l} \quad (3)$$

where  $\gamma$  is the discount factor,  $\lambda \in [0, 1]$  is the GAE parameter, and  $\delta_t = R(s_t, a_t) + \gamma V(s_{t+1}) - V(s_t)$  is the temporal-difference (TD) error. Here,  $R(s_t, a_t)$  is the reward at time step  $t$ , and  $V(s)$  is the value function. Since it is a common practice to use discount factor  $\gamma = 1.0$  in RLHF, to simplify our notation, we omit  $\gamma$  in later sections of this paper.

## 3 Challenges in Long-CoT RL for Reasoning Tasks

Long-CoT tasks present unique challenges to RL training, especially for methods that employ a value model to reduce variance. In this section, we systematically analyze the technical issues arising from sequence length dynamics, value function instability, and reward sparsity.

### 3.1 Value Model Bias over Long Sequences

As identified in VC-PPO [30], initializing the value model with a reward model introduces significant initialization bias. This positive bias arises from an objective mismatch between the two models. The reward model is trained to score on the <EOS> token, incentivizing it to assign lower scores to earlier tokens due to their incomplete context. In contrast, the value model estimates the expected cumulative reward for all tokens preceding <EOS> under a given policy. During early training phases, given the backward computation of GAE, there will be a positive bias at every timestep  $t$  that accumulates along the trajectory.

Another standard practice of using GAE with  $\lambda = 0.95$  might exacerbate this issue. The reward signal  $R(s_t, \text{<EOS>})$  at the termination token propagates backward as  $\lambda^{T-t} R(s_t, \text{<EOS>})$  to the  $t$ -th token. For long sequences where  $T - t \gg 1$ , this discounting reduces the effective reward signal to near zero. Consequently, value updates become almost entirely bootstrapped, relying on highly biased estimates that undermine the value model's role as a reliable variance-reduction baseline.

在此方程中， $H$  表示决策步骤的总数， $s_0$  是从数据集中采样的提示， $R(s_t, a_t)$  是从奖励函数中获得的基于 token 的奖励， $\beta$  是控制 KL 正则化强度的系数，而  $\pi_{\text{ref}}$  是初始化策略。

在传统的 RLHF 和大多数与 LLM 相关的任务中，奖励是稀疏的，仅在终端动作  $\omega$ ，即句子结束 token <eos> 时分配。

### 2.3 近端策略优化

PPO [21] 使用截断的替代目标来更新策略。其关键思想是在每次更新步骤中限制策略的变化，防止过大的策略更新导致不稳定。

设  $\pi_{\theta}(a|s)$  为参数化为  $\theta$  的策略， $\pi_{\text{old}}(a|s)$  为上一迭代中的旧策略。PPO 的替代目标函数定义为：

$$\mathcal{L}^{\text{CLIP}}(\theta) = \mathbb{E}_s \left[ \min \left( r_t(\theta) \hat{A}_t, \text{clip}(r_t(\theta), 1 - \epsilon, 1 + \epsilon) \hat{A}_t \right) \right] \quad (2)$$

其中  $r_t(\theta) = \frac{\pi_{\text{old}}(a_t|s_t)}{\pi_{\text{old}}(a_t|s_t)}$  是概率比， $\hat{A}_t$  是时间步  $t$  的估计优势， $\epsilon$  是控制截断范围的超参数。

广义优势估计 [20] 是一种在 PPO 中用来更准确估计优势函数的技术。它结合了多步引导来减少优势估计的方差。对于长度为  $T$  的轨迹，时间步  $t$  的优势估计  $\hat{A}_t$  计算为：

$$\hat{A}_t = \sum_{l=0}^{T-t-1} (\gamma \lambda)^l \delta_{t+l} \quad (3)$$

其中  $\gamma$  是折扣因子， $\lambda \in [0, 1]$  是 GAE 参数， $\delta_t = R(s_t, a_t) + \gamma V(s_{t+1}) - V(s_t)$  是时序差分（TD）误差。这里， $R(s_t, a_t)$  是时间步  $t$  的奖励， $V(s)$  是价值函数。由于在 RLHF 中常用的做法是使用折扣因子  $\gamma = 1.0$ ，为简化记号，本文后续部分将省略  $\gamma$ 。

## 3 长链式思维路径强化学习在推理任务中的挑战

长链式思维路径任务对强化学习训练带来了独特的挑战，特别是对于使用价值模型来减少方差的方法。在本节中，我们系统地分析了由序列长度动态、价值函数不稳定性和奖励稀疏性引发的技术问题。

### 3.1 长序列上的价值模型偏差

如VC-PPO中所指出的 [30]，用奖励模型初始化价值模型会引入显著的初始化偏差。这种正偏差来源于两个模型之间的目标不匹配。奖励模型被训练在<eos>标记上打分，激励其对较早的标记给予较低分数，因为对于这些标记的上下文不完整。相比之下，价值模型估计在给定策略下<eos>之前所有标记的预期累计奖励。在训练初期阶段，由于GAE的反向计算，每个时间步 $t$ 都会存在一个正偏差，并沿着轨迹累积。

使用 $\lambda = 0.95$ 的GAE的另一种常见做法可能会加剧这一问题。在终止标记处的奖励信号 $R(s_t, \text{<EOS>})$ 向后传播为 $\lambda^{T-t} R(s_t, \text{<EOS>})$ 到第 $t$ 个标记。对于长序列而言，当 $T - t \gg 1$ 时，这种折扣会将有效的奖励信号降低到接近于零。因此，价值更新几乎完全依赖于高度有偏差的估计，削弱了价值模型作为可靠的方差降低基线的作用。

4

(c) The second part of the English PDF of case 1.

(d) The second part of the Chinese PDF of case 1.

Figure 6: Case 1 demonstrates the performance of LaTeXTrans on the En-Zh task

## 1. Introduction

In recent years, Large Language Models (LLMs) have been undergoing rapid iteration and evolution (Anthropic, 2024; Google, 2024; OpenAI, 2024a), progressively diminishing the gap towards Artificial General Intelligence (AGI).

Recently, post-training has emerged as an important component of the full training pipeline. It has been shown to enhance accuracy on reasoning tasks, align with social values, and adapt to user preferences, all while requiring relatively minimal computational resources against pre-training. In the context of reasoning capabilities, OpenAI’s o1 (OpenAI, 2024b) series models were the first to introduce inference-time scaling by increasing the length of the Chain-of-Thought reasoning process. This approach has achieved significant improvements in various reasoning tasks, such as mathematics, coding, and scientific reasoning. However, the challenge of effective test-time scaling remains an open question for the research community. Several prior works have explored various approaches, including process-based reward models (Lightman et al., 2023; Uesato et al., 2022; Wang et al., 2023), reinforcement learning (Kumar et al., 2024), and search algorithms such as Monte Carlo Tree Search and Beam Search (Feng et al., 2024; Trinh et al., 2024; Xin et al., 2024). However, none of these methods has achieved general reasoning performance comparable to OpenAI’s o1 series models.

In this paper, we take the first step toward improving language model reasoning capabilities using pure reinforcement learning (RL). Our goal is to explore the potential of LLMs to develop reasoning capabilities without any supervised data, focusing on their self-evolution through a pure RL process. Specifically, we use DeepSeek-V3-Base as the base model and employ GRPO (Shao et al., 2024) as the RL framework to improve model performance in reasoning. During training, DeepSeek-R1-Zero naturally emerged with numerous powerful and interesting reasoning behaviors. After thousands of RL steps, DeepSeek-R1-Zero exhibits super performance on reasoning benchmarks. For instance, the pass@1 score on AIME 2024 increases from 15.6% to 71.0%, and with majority voting, the score further improves to 86.7%, matching the performance of OpenAI-o1-0912.

However, DeepSeek-R1-Zero encounters challenges such as poor readability, and language mixing. To address these issues and further enhance reasoning performance, we introduce DeepSeek-R1, which incorporates a small amount of cold-start data and a multi-stage training pipeline. Specifically, we begin by collecting thousands of cold-start data to fine-tune the DeepSeek-V3-Base model. Following this, we perform reasoning-oriented RL like DeepSeek-R1-Zero. Upon nearing convergence in the RL process, we create new SFT data through rejection sampling on the RL checkpoint, combined with supervised data from DeepSeek-V3 in domains such as writing, factual QA, and self-cognition, and then retrain the DeepSeek-V3-Base model. After fine-tuning with the new data, the checkpoint undergoes an additional RL process, taking into account prompts from all scenarios. After these steps, we obtained a checkpoint referred to as DeepSeek-R1, which achieves performance on par with OpenAI-o1-1217.

We further explore distillation from DeepSeek-R1 to smaller dense models. Using Qwen2.5-32B (Qwen, 2024b) as the base model, direct distillation from DeepSeek-R1 outperforms applying RL on it. This demonstrates that the reasoning patterns discovered by larger base models are crucial for improving reasoning capabilities. We open-source the distilled Qwen and Llama (Dubey et al., 2024) series. Notably, our distilled 14B model outperforms state-of-the-art open-source Qwen2.5-72B-Preview (Qwen, 2024a) by a large margin, and the distilled 32B and 70B models set a new record on the reasoning benchmarks among dense models.

3

(a) The first part of the English PDF of case 2.

• **Others:** DeepSeek-R1 also excels in a wide range of tasks, including creative writing, general question answering, editing, summarization, and more. It achieves an impressive length-controlled win-rate of 87.6% on AlpacaEval 2.0 and a win-rate of 92.3% on ArenaHard, showcasing its strong ability to intelligently handle non-exam-oriented queries. Additionally, DeepSeek-R1 demonstrates outstanding performance on tasks requiring long-context understanding, substantially outperforming DeepSeek-V3 on long-context benchmarks.

## 2. Approach

### 2.1. Overview

Previous work has heavily relied on large amounts of supervised data to enhance model performance. In this study, we demonstrate that reasoning capabilities can be significantly improved through large-scale reinforcement learning (RL), even without using supervised fine-tuning (SFT) as a cold start. Furthermore, performance can be further enhanced with the inclusion of a small amount of cold-start data. In the following sections, we present: (1) DeepSeek-R1-Zero, which applies RL directly to the base model without any SFT data, and (2) DeepSeek-R1, which applies RL starting from a checkpoint fine-tuned with thousands of long Chain-of-Thought (CoT) examples. (3) Distill the reasoning capability from DeepSeek-R1 to small dense models.

### 2.2. DeepSeek-R1-Zero: Reinforcement Learning on the Base Model

Reinforcement learning has demonstrated significant effectiveness in reasoning tasks, as evidenced by our previous works (Shao et al., 2024; Wang et al., 2023). However, these works heavily depended on supervised data, which are time-intensive to gather. In this section, we explore the potential of LLMs to develop reasoning capabilities **without any supervised data**, focusing on their self-evolution through a pure reinforcement learning process. We start with a brief overview of our RL algorithm, followed by the presentation of some exciting results, and hope this provides the community with valuable insights.

#### 2.2.1. Reinforcement Learning Algorithm

**Group Relative Policy Optimization.** In order to save the training costs of RL, we adopt Group Relative Policy Optimization (GRPO) (Shao et al., 2024), which foregoes the critic model that is typically the same size as the policy model, and estimates the baseline from group scores instead. Specifically, for each question  $q$ , GRPO samples a group of outputs  $\{o_1, o_2, \dots, o_G\}$  from the old policy  $\pi_{\theta_{\text{old}}}$  and then optimizes the policy model  $\pi_\theta$  by maximizing the following objective:

$$\mathcal{J}_{\text{GRPO}}(\theta) = \mathbb{E}[q \sim P(Q), \{o_i\}_{i=1}^G \sim \pi_{\theta_{\text{old}}}(Q|q)]$$

$$\frac{1}{G} \sum_{i=1}^G \left( \min \left( \frac{\pi_\theta(o_i|q)}{\pi_{\theta_{\text{old}}}(o_i|q)} A_i, \text{clip} \left( \frac{\pi_\theta(o_i|q)}{\pi_{\theta_{\text{old}}}(o_i|q)}, 1 - \epsilon, 1 + \epsilon \right) A_i \right) - \beta \text{D}_{\text{KL}}(\pi_\theta \parallel \pi_{\text{ref}}) \right), \quad (1)$$

$$\text{D}_{\text{KL}}(\pi_\theta \parallel \pi_{\text{ref}}) = \frac{\pi_\theta(o_i|q)}{\pi_{\theta_{\text{old}}}(o_i|q)} - \log \frac{\pi_\theta(o_i|q)}{\pi_{\theta_{\text{old}}}(o_i|q)} - 1, \quad (2)$$

where  $\epsilon$  and  $\beta$  are hyper-parameters, and  $A_i$  is the advantage, computed using a group of rewards  $\{r_1, r_2, \dots, r_G\}$  corresponding to the outputs within each group:

$$A_i = \frac{r_i - \text{mean}(\{r_1, r_2, \dots, r_G\})}{\text{std}(\{r_1, r_2, \dots, r_G\})}. \quad (3)$$

5

(c) The second part of the English PDF of case 2.

## 1. 介绍

近年来，大型语言模型 (LLMs) 正在经历快速迭代和演变 (Anthropic, 2024; Google, 2024; OpenAI, 2024a)，逐步缩小与人工通用智能 (AGI) 的差距。

最近，后训练已成为完整训练流程中的重要组成部分。研究表明，它能够增强推理任务的准确性，符合社会价值观，并适应用户偏好，同时与预训练相比需要相对较少的计算资源。在推理能力的背景下，OpenAI 的 o1 系列模型首次通过增加链式思维推理过程的长度，引入了推理时间缩放。这种方法在各种推理任务中取得了显著改进，如数学、编码和科学推理。然而，有效的测试时间缩放仍然是研究界的一个开放问题。一些先前的工作探索了各种方法，包括基于过程的奖励模型 (Lightman et al., 2023; Uesato et al., 2022; Wang et al., 2023)，强化学习 (Kumar et al., 2024) 和搜索算法，如蒙特卡洛树搜索和束搜索 (Feng et al., 2024; Trinh et al., 2024; Xin et al., 2024)。然而，这些方法都未能实现与 OpenAI 的 o1 系列模型相媲美的通用推理性能。

在本文中，我们迈出了使用纯强化学习 (RL) 提高语言模型推理能力的第一步。我们的目标是探索 LLMs 在不使用任何监督数据的情况下发展推理能力的潜力，重点在于通过纯 RL 过程进行自我进化。具体来说，我们使用 DeepSeek-V3-Base 作为基础模型，并采用 GRPO (Shao et al., 2024) 作为 RL 框架来提高模型在推理中的性能。在训练过程中，DeepSeek-R1-Zero 自然涌现出许多强大且有趣的推理行为。经过数千次 RL 步骤后，DeepSeek-R1-Zero 在推理基准测试中表现出超强性能。例如，AIME 2024 的 pass@1 得分从 15.6% 提高到 71.0%，并且通过多数投票，得分进一步提高到 86.7%，与 OpenAI-o1-0912 的性能相当。

然而，DeepSeek-R1-Zero 遇到了一些挑战，如可读性差和语言混合。为了解决这些问题并进一步提高推理性能，我们引入了 DeepSeek-R1，其中包含少量冷启动数据和多阶段训练流程。具体来说，我们首先收集数千条冷启动数据来微调 DeepSeek-V3-Base 模型。随后，我们进行类似于 DeepSeek-R1-Zero 的推理导向 RL。当 RL 过程接近收敛时，我们通过 RL 检查点上的拒绝抽样创建新的 SFT 数据，并结合 DeepSeek-V3 在写作、事实问答和自我认知等领域的监督数据，然后重新训练 DeepSeek-V3-Base 模型。在用新数据微调后，检查点经过额外的 RL 过程，考虑所有场景的提示，经过这些步骤，我们获得了一个被称为 DeepSeek-R1 的检查点，其性能与 OpenAI-o1-1217 相当。

我们进一步探索了从 DeepSeek-R1 到更小的密集模型的蒸馏。使用 Qwen2.5-32B (Qwen, 2024b) 作为基础模型，直接从 DeepSeek-R1 蒸馏优于在其上应用 RL。这表明较大基础模型发现的推理模式对于提高推理能力至关重要。我们开源了蒸馏的 Qwen 和 Llama (Dubey et al., 2024) 系列。值得注意的是，我们蒸馏的 14B 模型在推理基准测试中远超过最先进的开源 Qwen2.5-72B-Preview (Qwen, 2024a)，蒸馏的 32B 和 70B 模型在密集模型中创下了推理基准测试的新纪录。

3

(b) The first part of the Chinese PDF of case 2.

• **其他:** DeepSeek-R1 在广泛的任务中也表现出色，包括创意写作、一般问答、编辑、总结等。在 AlpacaEval 2.0 上取得了 87.6% 的长度控制胜率，在 ArenaHard 上取得了 92.3% 的胜率，展现了其智能处理非考试导向查询的强大能力。此外，DeepSeek-R1 在需要长上下文理解的任务中表现出色，在长上下文基准测试中显著超越了 DeepSeek-V3。

## 2. 方法

### 2.1. 概述

以往的研究大量依赖监督数据来提升模型性能。在本研究中，我们展示了即使不使用监督微调 (SFT) 作为冷启动，通过大规模强化学习 (RL) 可以显著提高推理能力。此外，加入少量冷启动数据可以进一步提升性能。在接下来的部分中，我们介绍：(1) DeepSeek-R1-Zero，它直接将 RL 应用于基础模型而不使用任何 SFT 数据，(2) DeepSeek-R1，它从经过数千个长链式思维 (CoT) 示例微调的检查点开始应用 RL，(3) 将 DeepSeek-R1 的推理能力提炼到小型稠密模型中。

### 2.2. DeepSeek-R1-Zero：基础模型上的强化学习

强化学习在推理任务中显示出显著的效果。这在我们之前的工作中已经得到了证实 (Shao et al., 2024; Wang et al., 2023)。然而，这些工作在很大程度上依赖于监督数据，而这些数据的收集非常耗时。在本节中，我们探索 LLMs 在 **没有任何监督数据** 的情况下发展推理能力的潜力，重点关注它们通过纯粹的强化学习过程实现自我进化。我们首先简要概述我们的 RL 算法，然后介绍一些令人兴奋的结果，并希望这能为社区提供有价值的见解。

#### 2.2.1. 强化学习算法

**群组相对策略优化。** 为了节省强化学习的训练成本，我们采用群组相对策略优化 (GRPO) (Shao et al., 2024)。该方法放弃了通常与策略模型大小相同的评论模型，而是通过群组评分来估计基线。具体来说，对于每个问题  $q$ ，GRPO 从旧策略  $\pi_{\theta_{\text{old}}}$  中采样一组输出  $\{o_1, o_2, \dots, o_G\}$ ，然后通过最大化以下目标来优化策略模型  $\pi_\theta$ ：

$$\mathcal{J}_{\text{GRPO}}(\theta) = \mathbb{E}[q \sim P(Q), \{o_i\}_{i=1}^G \sim \pi_{\theta_{\text{old}}}(Q|q)]$$

$$\frac{1}{G} \sum_{i=1}^G \left( \min \left( \frac{\pi_\theta(o_i|q)}{\pi_{\theta_{\text{old}}}(o_i|q)} A_i, \text{clip} \left( \frac{\pi_\theta(o_i|q)}{\pi_{\theta_{\text{old}}}(o_i|q)}, 1 - \epsilon, 1 + \epsilon \right) A_i \right) - \beta \text{D}_{\text{KL}}(\pi_\theta \parallel \pi_{\text{ref}}) \right), \quad (1)$$

$$\text{D}_{\text{KL}}(\pi_\theta \parallel \pi_{\text{ref}}) = \frac{\pi_\theta(o_i|q)}{\pi_{\theta_{\text{old}}}(o_i|q)} - \log \frac{\pi_\theta(o_i|q)}{\pi_{\theta_{\text{old}}}(o_i|q)} - 1, \quad (2)$$

其中  $\epsilon$  和  $\beta$  是超参数， $A_i$  是优势，通过使用对应于每个群组内输出的一组奖励  $\{r_1, r_2, \dots, r_G\}$  来计算：

$$A_i = \frac{r_i - \text{mean}(\{r_1, r_2, \dots, r_G\})}{\text{std}(\{r_1, r_2, \dots, r_G\})}. \quad (3)$$

5

(d) The second part of the Chinese PDF of case 2.

Figure 7: Case 2 demonstrates the performance of LaTeXTrans on the En-Zh task

In the multi-snapshot scenario, the forward  $T$ -measurement process is described as

$$\mathbf{Y} = \mathbf{A} \cdot \mathbf{S} + \mathbf{N}, \quad (9)$$

where  $\mathbf{Y} = [\mathbf{y}(1), \dots, \mathbf{y}(T)] \in \mathbb{C}^{M \times T}$  is the matrix of received signals across  $T$  time snapshots,  $\mathbf{S} = [\mathbf{s}_1, \dots, \mathbf{s}_T] \in \mathbb{C}^{L \times T}$  denotes the source signal matrix, and  $\mathbf{N} \in \mathbb{C}^{M \times T}$  represents the noise.

#### B. Classical 2D MUSIC Algorithm

The MUSIC algorithm is widely used for AoA estimation through eigenvalue decomposition. Based on the model in (9), the covariance matrix of the received signals is given by

$$\begin{aligned} \mathbf{R} &= E[\mathbf{Y}\mathbf{Y}^H] \\ &= \mathbf{A}\mathbf{R}_s\mathbf{A}^H + \sigma^2\mathbf{I}, \end{aligned} \quad (10)$$

where  $\mathbf{R}_s = E[\mathbf{S}\mathbf{S}^H]$  is the correlation matrix of the source signals. The eigenvectors of  $\mathbf{R}$  associated with the largest  $D$  eigenvalues span the signal subspace  $E_s$ , while the remaining eigenvectors span the noise subspace  $E_N$ . The 2D MUSIC AoA pseudo-spectrum is defined as

$$P_{\text{MUSIC}}(\theta, \phi) = \frac{\mathbf{a}^H(\theta, \phi)\mathbf{a}(\theta, \phi)}{\mathbf{a}^H(\theta, \phi)\mathbf{E}_N\mathbf{E}_N^H\mathbf{a}(\theta, \phi)}. \quad (11)$$

The angles corresponding to the peaks in this pseudo-spectrum provide estimates of the directions of the incident signals.

#### C. 1-SSMUSIC for 3D AoA

In contrast to 2D AoA estimation, 3D AoA estimation demands significantly higher computational complexity. Moreover, 3D localization tasks are further challenged by the increased severity of multipath propagation. A well-known limitation of subspace-based methods is their degraded performance in the presence of correlated sources, primarily due to rank deficiency in the covariance matrix. A notable solution to mitigate this issue is the spatial smoothing technique.

We now present an improved MUSIC algorithm with 2D spatial smoothing, referred to as 1-SSMUSIC, designed for URAs. Based on (9), the  $(m_1, m_2)$ -th smoothed subarray of size  $M_1 \times M_2$  is formally expressed as

$$\mathbf{Y}_{m_1 m_2} = \mathbf{A}_1 \mathbf{D}_x^{m_1-1} \mathbf{D}_y^{m_2-1} \mathbf{S} + \mathbf{N}_{m_1 m_2}, \quad (12)$$

where

$$\begin{aligned} \mathbf{D}_x &= \text{diag}[u(\theta_1, \phi_1), \dots, u(\theta_L, \phi_L)], \\ \mathbf{D}_y &= \text{diag}[v(\theta_1, \phi_1), \dots, v(\theta_L, \phi_L)], \end{aligned} \quad (13)$$

Here  $\mathbf{N}_{m_1 m_2}$  is the noise matrix at the  $(m_1, m_2)$ -th subarray and  $\mathbf{A}_1 = [\mathbf{a}_1(\theta_1, \phi_1), \mathbf{a}_1(\theta_2, \phi_2), \dots, \mathbf{a}_1(\theta_L, \phi_L)]$  is the steering matrix, where each  $\mathbf{a}_1(\theta_i, \phi_i)$  is given by

$$\begin{aligned} \mathbf{a}_1(\theta_i, \phi_i) &= \mathbf{a}_{x, M_1}(\theta_i, \phi_i) \otimes \mathbf{a}_{y, M_2}(\theta_i, \phi_i), \\ \mathbf{a}_{x, M_1}(\theta, \phi) &= [1 \quad u \quad \dots \quad u^{M_1-1}]^T, \\ \mathbf{a}_{y, M_2}(\theta, \phi) &= [1 \quad v \quad \dots \quad v^{M_2-1}]^T. \end{aligned} \quad (14)$$

(a) The first part of the English PDF of case 3.

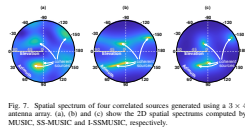


Fig. 7. Spatial spectrum of four correlated sources generated using a  $3 \times 4$  antenna array. (a), (b) and (c) show the 3D spatial spectrum computed by MUSIC, SS-MUSIC and 1-SSMUSIC, respectively.

of correlated signals while mitigating the effects of rank deficiency.

By examining (16) and (18), we observe that the number of forward-only smoothed subarrays, denoted by  $H$ , determines the maximum number of resolvable correlated sources, whereas forward-backward smoothing effectively doubles this limit to  $2H$ . In typical indoor environments, where the number of multipath components is usually fewer than five [13], (17), a single forward-backward smoothing operation ( $H=2$ ) can decorrelate signals from up to four distinct angles.

We now present a comparative evaluation of conventional MUSIC, MUSIC with forward-only spatial smoothing (SS-MUSIC), and the proposed 1-SSMUSIC for estimating the angles of four correlated signals under identical conditions. The URA consists of  $3 \times 4$  antennas. Four correlated signal sources emit continuous signals with an SNR of 15 dB, arriving from the following angles:  $(21.8^\circ, 90^\circ)$ ,  $(32^\circ, 56^\circ)$ ,  $(15^\circ, -60^\circ)$  and  $(60^\circ, -150^\circ)$ , respectively. The spatial spectra are illustrated in Fig. 7, from which it is evident that the proposed 1-SSMUSIC outperforms the other methods. The estimated AoAs using 1-SSMUSIC are  $(21.8^\circ, 90.8^\circ)$ ,  $(32.4^\circ, 57.2^\circ)$ ,  $(16.4^\circ, -59.6^\circ)$  and  $(60.2^\circ, -150.6^\circ)$ , respectively. In comparison, while SS-MUSIC is capable of estimating correlated signals, it exhibits notably lower resolution. Its estimated AoAs are  $(22.8^\circ, 82.2^\circ)$ ,  $(37.2^\circ, 50.8^\circ)$ ,  $(15.2^\circ, -62^\circ)$  and  $(58.8^\circ, -149.6^\circ)$ . The standard MUSIC algorithm, by contrast, fails to resolve the correlated sources, resulting in an ambiguous and inaccurate AoA spectrum.

#### D. Closest Geometric Point Estimation

With AoA estimations obtained from multiple URAs distributed across space, the specific location of the signal source can be determined. Ideally, the estimated AoA vectors intersect at the true position of the source. However, due to measurement errors, a robust closest-point estimation algorithm is required to approximate the actual point of intersection. The proposed geometric positioning (GP) method first identifies the closest points between each pair of AoAs, as illustrated in Stage 1 of Fig. 8. The final position estimate is then computed as the mean of these closest points.

Let  $\mathbf{l}_i$  denote the estimated arrival ray associated with the  $i$ -th URA. Each ray can be represented by a parametric equation

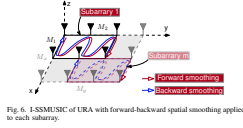


Fig. 6. 1-SSMUSIC of URA with forward-backward spatial smoothing applied to each subarray.

Using (12), we can reformulate the expression in (10). The covariance matrix of the  $(m_1, m_2)$ -th subarray is therefore given by

$$\begin{aligned} \mathbf{R}_{m_1 m_2} &= \mathbf{A}_1 \mathbf{D}_x^{m_1-1} \mathbf{D}_y^{m_2-1} \mathbf{R}_s (\mathbf{D}_x^{m_1-1})^H \\ &\quad \times (\mathbf{D}_y^{m_2-1})^H \mathbf{A}_1^H + \sigma^2 \mathbf{I}. \end{aligned} \quad (15)$$

In the spatial smoothing scheme, the forward smoothed covariance matrix  $\mathbf{R}^f$  is obtained by averaging the covariance matrices of all forward subarrays, yielding

$$\mathbf{R}^f = \frac{1}{H_x H_y} \sum_{m_1=1}^{H_x} \sum_{m_2=1}^{H_y} \mathbf{R}_{m_1 m_2} = \mathbf{A}_1 \mathbf{R}_s^f \mathbf{A}_1^H + \sigma^2 \mathbf{I}, \quad (16)$$

where  $H_x = M_1 - M_f + 1$  and  $H_y = M_2 - M_f + 1$ . Similarly, we denote the forward-smoothed source covariance matrix by  $\mathbf{R}_s^f$ , which is defined by

$$\begin{aligned} \mathbf{R}_s^f &= \frac{1}{H_x H_y} \sum_{m_1=1}^{H_x} \sum_{m_2=1}^{H_y} \mathbf{D}_x^{m_1-1} \mathbf{D}_y^{m_2-1} \mathbf{R}_s \\ &\quad \times (\mathbf{D}_x^{m_1-1})^H (\mathbf{D}_y^{m_2-1})^H. \end{aligned} \quad (17)$$

The spatially smoothed covariance matrix enables the application of eigenstructure-based methods for AoA estimation, even in the presence of coherent signals.

One limitation of the spatial smoothing algorithm is its tendency to reduce the effective array aperture, which may degrade sensing performance [17]. To mitigate this issue, we introduce a forward-backward spatial smoothing scheme for URAs, as illustrated in Fig. 6. This bidirectional smoothing approach preserves the aperture size by exploiting the conjugate symmetry property of the covariance matrix.

Mathematically, the forward-backward spatially smoothed covariance matrix is expressed as

$$\mathbf{R}_x = \frac{1}{2} (\mathbf{R}^f + \mathbf{I}_x (\mathbf{R}^f)^H \mathbf{I}_x), \quad (18)$$

where  $(\mathbf{R}^f)^H$  is the conjugate for matrix  $\mathbf{R}^f$ , and

$$\mathbf{I}_x = \begin{bmatrix} 0 & \dots & 0 & 1 \\ 0 & \dots & 1 & 0 \\ \vdots & \vdots & \vdots & \vdots \\ 1 & \dots & 0 & 0 \end{bmatrix}_{M_1 \times M_1}. \quad (19)$$

By computing the pseudo-spectrum in (11) using this smoothed covariance matrix, we enable accurate estimation

每列对应一个不同的到达方向。向量  $\mathbf{a}(t) \in \mathbb{C}^{L \times 1}$  包含信号， $\epsilon(t)$  是零均值方差为  $\sigma^2$  的复高斯噪声向量。

在多次快照场景中，前向  $T$  测量过程描述为

$$\mathbf{Y} = \mathbf{A} \cdot \mathbf{S} + \mathbf{N}, \quad (9)$$

其中  $\mathbf{Y} = [\mathbf{y}(1), \dots, \mathbf{y}(T)] \in \mathbb{C}^{M \times T}$  是跨  $T$  时间快照的接收信号矩阵， $\mathbf{S} = [\mathbf{s}_1, \dots, \mathbf{s}_T] \in \mathbb{C}^{L \times T}$  表示源信号矩阵， $\mathbf{N} \in \mathbb{C}^{M \times T}$  代表噪声。

#### B. 经典二维 MUSIC 算法

MUSIC 算法广泛用于通过特征值分解进行到达角估计。基于模型 (9)，接收到的信号的协方差矩阵表示为

$$\begin{aligned} \mathbf{R} &= E[\mathbf{Y}\mathbf{Y}^H] \\ &= \mathbf{A}\mathbf{R}_s\mathbf{A}^H + \sigma^2\mathbf{I}, \end{aligned} \quad (10)$$

其中  $\mathbf{R}_s = E[\mathbf{S}\mathbf{S}^H]$  为源信号的相关矩阵。与最大  $D$  个特征值相关的  $\mathbf{R}$  的特征向量组成信号子空间  $E_s$ ，而其余特征向量组成噪声子空间  $E_N$ 。二维 MUSIC 到达角伪谱定义为

$$P_{\text{MUSIC}}(\theta, \phi) = \frac{\mathbf{a}^H(\theta, \phi)\mathbf{a}(\theta, \phi)}{\mathbf{a}^H(\theta, \phi)\mathbf{E}_N\mathbf{E}_N^H\mathbf{a}(\theta, \phi)}. \quad (11)$$

该伪谱中峰值对应的角度提供了入射信号方向的估计。

#### C. 用于三维到达角的 1-SSMUSIC

与二维到达角估计相比，三维到达角估计需要显著更高的计算复杂度。此外，三维定位任务还面临多径传播严重性的增加。一种众所周知的基于子空间的方法的局限性是在存在相关源的情况下性能下降，主要是由于协方差矩阵的秩不足。一个显著的解决方案是空间平滑技术。

我们现在介绍一种改进的 MUSIC 算法，采用二维空间平滑，称为 1-SSMUSIC，专为 URA 设计。基于 (9)，大小为  $M_1 \times M_2$  的第  $(m_1, m_2)$  个平滑子阵形式上表示为

$$\mathbf{Y}_{m_1 m_2} = \mathbf{A}_1 \mathbf{D}_x^{m_1-1} \mathbf{D}_y^{m_2-1} \mathbf{S} + \mathbf{N}_{m_1 m_2}, \quad (12)$$

其中

$$\begin{aligned} \mathbf{D}_x &= \text{diag}[u(\theta_1, \phi_1), \dots, u(\theta_L, \phi_L)], \\ \mathbf{D}_y &= \text{diag}[v(\theta_1, \phi_1), \dots, v(\theta_L, \phi_L)], \end{aligned} \quad (13)$$

(b) The first part of the Chinese PDF of case 3.

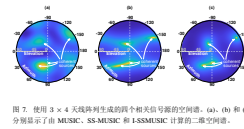


Fig. 7. Spatial spectrum of four correlated sources generated using a  $3 \times 4$  antenna array. (a), (b) and (c) show the 3D spatial spectrum computed by MUSIC, SS-MUSIC and 1-SSMUSIC, respectively.

of correlated signals while mitigating the effects of rank deficiency.

By examining (16) and (18), we observe that the number of forward-only smoothed subarrays, denoted by  $H$ , determines the maximum number of resolvable correlated sources, whereas forward-backward smoothing effectively doubles this limit to  $2H$ . In typical indoor environments, where the number of multipath components is usually fewer than five [13], (17), a single forward-backward smoothing operation ( $H=2$ ) can decorrelate signals from up to four distinct angles.

We now present a comparative evaluation of conventional MUSIC, MUSIC with forward-only spatial smoothing (SS-MUSIC), and the proposed 1-SSMUSIC for estimating the angles of four correlated signals under identical conditions. The URA consists of  $3 \times 4$  antennas. Four correlated signal sources emit continuous signals with an SNR of 15 dB, arriving from the following angles:  $(21.8^\circ, 90^\circ)$ ,  $(32^\circ, 56^\circ)$ ,  $(15^\circ, -60^\circ)$  and  $(60^\circ, -150^\circ)$ , respectively. The spatial spectra are illustrated in Fig. 7, from which it is evident that the proposed 1-SSMUSIC outperforms the other methods. The estimated AoAs using 1-SSMUSIC are  $(21.8^\circ, 90.8^\circ)$ ,  $(32.4^\circ, 57.2^\circ)$ ,  $(16.4^\circ, -59.6^\circ)$  and  $(60.2^\circ, -150.6^\circ)$ , respectively. In comparison, while SS-MUSIC is capable of estimating correlated signals, it exhibits notably lower resolution. Its estimated AoAs are  $(22.8^\circ, 82.2^\circ)$ ,  $(37.2^\circ, 50.8^\circ)$ ,  $(15.2^\circ, -62^\circ)$  and  $(58.8^\circ, -149.6^\circ)$ . The standard MUSIC algorithm, by contrast, fails to resolve the correlated sources, resulting in an ambiguous and inaccurate AoA spectrum.

#### D. Closest Geometric Point Estimation

With AoA estimations obtained from multiple URAs distributed across space, the specific location of the signal source can be determined. Ideally, the estimated AoA vectors intersect at the true position of the source. However, due to measurement errors, a robust closest-point estimation algorithm is required to approximate the actual point of intersection. The proposed geometric positioning (GP) method first identifies the closest points between each pair of AoAs, as illustrated in Stage 1 of Fig. 8. The final position estimate is then computed as the mean of these closest points.

Let  $\mathbf{l}_i$  denote the estimated arrival ray associated with the  $i$ -th URA. Each ray can be represented by a parametric equation

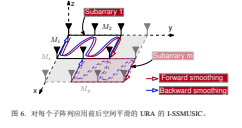


Fig. 6. 1-SSMUSIC of URA with forward-backward spatial smoothing applied to each subarray.

Using (12), we can reformulate the expression in (10). The covariance matrix of the  $(m_1, m_2)$ -th subarray is therefore given by

$$\begin{aligned} \mathbf{R}_{m_1 m_2} &= \mathbf{A}_1 \mathbf{D}_x^{m_1-1} \mathbf{D}_y^{m_2-1} \mathbf{R}_s (\mathbf{D}_x^{m_1-1})^H \\ &\quad \times (\mathbf{D}_y^{m_2-1})^H \mathbf{A}_1^H + \sigma^2 \mathbf{I}. \end{aligned} \quad (15)$$

In the spatial smoothing scheme, the forward smoothed covariance matrix  $\mathbf{R}^f$  is obtained by averaging the covariance matrices of all forward subarrays, yielding

$$\mathbf{R}^f = \frac{1}{H_x H_y} \sum_{m_1=1}^{H_x} \sum_{m_2=1}^{H_y} \mathbf{R}_{m_1 m_2} = \mathbf{A}_1 \mathbf{R}_s^f \mathbf{A}_1^H + \sigma^2 \mathbf{I}, \quad (16)$$

where  $H_x = M_1 - M_f + 1$  and  $H_y = M_2 - M_f + 1$ . Similarly, we denote the forward-smoothed source covariance matrix by  $\mathbf{R}_s^f$ , which is defined by

$$\begin{aligned} \mathbf{R}_s^f &= \frac{1}{H_x H_y} \sum_{m_1=1}^{H_x} \sum_{m_2=1}^{H_y} \mathbf{D}_x^{m_1-1} \mathbf{D}_y^{m_2-1} \mathbf{R}_s \\ &\quad \times (\mathbf{D}_x^{m_1-1})^H (\mathbf{D}_y^{m_2-1})^H. \end{aligned} \quad (17)$$

The spatially smoothed covariance matrix enables the application of eigenstructure-based methods for AoA estimation, even in the presence of coherent signals.

One limitation of the spatial smoothing algorithm is its tendency to reduce the effective array aperture, which may degrade sensing performance [17]. To mitigate this issue, we introduce a forward-backward spatial smoothing scheme for URAs, as illustrated in Fig. 6. This bidirectional smoothing approach preserves the aperture size by exploiting the conjugate symmetry property of the covariance matrix.

Mathematically, the forward-backward spatially smoothed covariance matrix is expressed as

$$\mathbf{R}_x = \frac{1}{2} (\mathbf{R}^f + \mathbf{I}_x (\mathbf{R}^f)^H \mathbf{I}_x), \quad (18)$$

where  $(\mathbf{R}^f)^H$  is the conjugate for matrix  $\mathbf{R}^f$ , and

$$\mathbf{I}_x = \begin{bmatrix} 0 & \dots & 0 & 1 \\ 0 & \dots & 1 & 0 \\ \vdots & \vdots & \vdots & \vdots \\ 1 & \dots & 0 & 0 \end{bmatrix}_{M_1 \times M_1}. \quad (19)$$

By computing the pseudo-spectrum in (11) using this smoothed covariance matrix, we enable accurate estimation

(c) The second part of the English PDF of case 3.

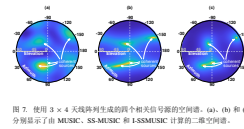


Fig. 7. Spatial spectrum of four correlated sources generated using a  $3 \times 4$  antenna array. (a), (b) and (c) show the 3D spatial spectrum computed by MUSIC, SS-MUSIC and 1-SSMUSIC, respectively.

of correlated signals while mitigating the effects of rank deficiency.

By examining (16) and (18), we observe that the number of forward-only smoothed subarrays, denoted by  $H$ , determines the maximum number of resolvable correlated sources, whereas forward-backward smoothing effectively doubles this limit to  $2H$ . In typical indoor environments, where the number of multipath components is usually fewer than five [13], (17), a single forward-backward smoothing operation ( $H=2$ ) can decorrelate signals from up to four distinct angles.

We now present a comparative evaluation of conventional MUSIC, MUSIC with forward-only spatial smoothing (SS-MUSIC), and the proposed 1-SSMUSIC for estimating the angles of four correlated signals under identical conditions. The URA consists of  $3 \times 4$  antennas. Four correlated signal sources emit continuous signals with an SNR of 15 dB, arriving from the following angles:  $(21.8^\circ, 90^\circ)$ ,  $(32^\circ, 56^\circ)$ ,  $(15^\circ, -60^\circ)$  and  $(60^\circ, -150^\circ)$ , respectively. The spatial spectra are illustrated in Fig. 7, from which it is evident that the proposed 1-SSMUSIC outperforms the other methods. The estimated AoAs using 1-SSMUSIC are  $(21.8^\circ, 90.8^\circ)$ ,  $(32.4^\circ, 57.2^\circ)$ ,  $(16.4^\circ, -59.6^\circ)$  and  $(60.2^\circ, -150.6^\circ)$ , respectively. In comparison, while SS-MUSIC is capable of estimating correlated signals, it exhibits notably lower resolution. Its estimated AoAs are  $(22.8^\circ, 82.2^\circ)$ ,  $(37.2^\circ, 50.8^\circ)$ ,  $(15.2^\circ, -62^\circ)$  and  $(58.8^\circ, -149.6^\circ)$ . The standard MUSIC algorithm, by contrast, fails to resolve the correlated sources, resulting in an ambiguous and inaccurate AoA spectrum.

#### D. Closest Geometric Point Estimation

With AoA estimations obtained from multiple URAs distributed across space, the specific location of the signal source can be determined. Ideally, the estimated AoA vectors intersect at the true position of the source. However, due to measurement errors, a robust closest-point estimation algorithm is required to approximate the actual point of intersection. The proposed geometric positioning (GP) method first identifies the closest points between each pair of AoAs, as illustrated in Stage 1 of Fig. 8. The final position estimate is then computed as the mean of these closest points.

Let  $\mathbf{l}_i$  denote the estimated arrival ray associated with the  $i$ -th URA. Each ray can be represented by a parametric equation

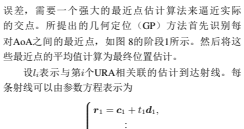


Fig. 7. Spatial spectrum of four correlated sources generated using a  $3 \times 4$  antenna array. (a), (b) and (c) show the 3D spatial spectrum computed by MUSIC, SS-MUSIC and 1-SSMUSIC, respectively.

of correlated signals while mitigating the effects of rank deficiency.

By examining (16) and (18), we observe that the number of forward-only smoothed subarrays, denoted by  $H$ , determines the maximum number of resolvable correlated sources, whereas forward-backward smoothing effectively doubles this limit to  $2H$ . In typical indoor environments, where the number of multipath components is usually fewer than five [13], (17), a single forward-backward smoothing operation ( $H=2$ ) can decorrelate signals from up to four distinct angles.

We now present a comparative evaluation of conventional MUSIC, MUSIC with forward-only spatial smoothing (SS-MUSIC), and the proposed 1-SSMUSIC for estimating the angles of four correlated signals under identical conditions. The URA consists of  $3 \times 4$  antennas. Four correlated signal sources emit continuous signals with an SNR of 15 dB, arriving from the following angles:  $(21.8^\circ, 90^\circ)$ ,  $(32^\circ, 56^\circ)$ ,  $(15^\circ, -60^\circ)$  and  $(60^\circ, -150^\circ)$ , respectively. The spatial spectra are illustrated in Fig. 7, from which it is evident that the proposed 1-SSMUSIC outperforms the other methods. The estimated AoAs using 1-SSMUSIC are  $(21.8^\circ, 90.8^\circ)$ ,  $(32.4^\circ, 57.2^\circ)$ ,  $(16.4^\circ, -59.6^\circ)$  and  $(60.2^\circ, -150.6^\circ)$ , respectively. In comparison, while SS-MUSIC is capable of estimating correlated signals, it exhibits notably lower resolution. Its estimated AoAs are  $(22.8^\circ, 82.2^\circ)$ ,  $(37.2^\circ, 50.8^\circ)$ ,  $(15.2^\circ, -62^\circ)$  and  $(58.8^\circ, -149.6^\circ)$ . The standard MUSIC algorithm, by contrast, fails to resolve the correlated sources, resulting in an ambiguous and inaccurate AoA spectrum.

#### D. Closest Geometric Point Estimation

With AoA estimations obtained from multiple URAs distributed across space, the specific location of the signal source can be determined. Ideally, the estimated AoA vectors intersect at the true position of the source. However, due to measurement errors, a robust closest-point estimation algorithm is required to approximate the actual point of intersection. The proposed geometric positioning (GP) method first identifies the closest points between each pair of AoAs, as illustrated in Stage 1 of Fig. 8. The final position estimate is then computed as the mean of these closest points.

Let  $\mathbf{l}_i$  denote the estimated arrival ray associated with the  $i$ -th URA. Each ray can be represented by a parametric equation

(c) The second part of the English PDF of case 3.

(d) The second part of the Chinese PDF of case 3.

Figure 8: Case 3 demonstrates the performance of LaTeXTrans on the En-Zh task

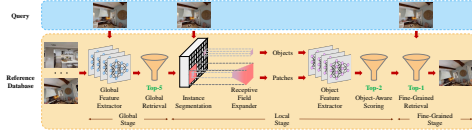


Figure 2. The AirRoom coarse-to-fine pipeline. The pipeline begins with the Global Feature Extractor, which captures global context features to retrieve the top-5 reference images. Instance segmentation then generates object masks, followed by the Receptive Field Expander, which extracts object patches. The Object Feature Extractor processes both object and patch features. The Object-Aware Scoring module narrows the selection to the top-2 candidates, and Fine-Grained Retrieval identifies the most suitable reference image.

However, the high performance of most VPR approaches is largely attributed to large-scale training on VPR-specific datasets [18]. Collecting extensive data for outdoor scenes is relatively straightforward due to natural variations in day-light, weather, and seasons. However, such data collection is more challenging in indoor rooms, making large-scale training on indoor datasets difficult and potentially limiting their effectiveness. Our approach effectively tackles this challenge by focusing on object-oriented feature representations, allowing us to leverage mature, pre-trained models for object feature learning. This design enables AirRoom to deliver robust performance without requiring any additional training or fine-tuning on specific datasets.

### 3. Proposed Approach

We propose a simple yet highly effective pipeline. AirRoom, for room reidentification that leverages multi-level object-oriented information, as shown in Figure 2. We will now systematically introduce each module of the pipeline, following the sequence of stages in which they are executed.

#### 3.1. Global Stage

In this stage, we utilize the Global Feature Extractor to capture global context features, which are derived from the collective presence of objects within the room. These features are then used for Global Retrieval, coarsely selecting semantically similar candidate rooms from the database.

##### 3.1.1. Global Feature Extractor

Indoor rooms exhibit fewer variations compared to outdoor environments. They lack diverse topographies, such as aerial, subterranean, or underwater features, and do not experience temporal changes like day-night or seasonal variations. Consequently, collecting large datasets for each indoor room is challenging, complicating large-scale training as seen in many VPR methods [1, 3, 13].

However, indoor rooms are inherently rich in objects,

each contributing to the room’s overall semantic context. By leveraging this global context information, we can refine the reference search to specifically focus on rooms with similar semantic features to those in the query image. For this purpose, we prefer backbones pretrained on large image datasets, as they provide strong generalizability and effectively capture informative global context features [17]. Our model selections, therefore, include pretrained CNN-based models such as ResNet [14] and transformer-based self-supervised models like DINOv2 [25].

##### 3.1.2. Global Retrieval

Using the Global Feature Extractor, we extract global context features for  $M$  query and  $N$  reference images. Let  $Q \in \mathbb{R}^{M \times D}$  and  $R \in \mathbb{R}^{N \times D}$  denote the query and reference features, respectively, where  $D$  is the feature dimension. The cosine similarity matrix  $S$  is then computed as:

$$S_{ij} = \frac{Q_i \cdot R_j}{\|Q_i\| \|R_j\|} \quad (1)$$

For each query, we select the top-5 most similar reference candidates using the following formula:

$$\text{Top}_5(S_{i,:}) = \text{arg-sort}(-S_{i,:})[:5], \quad (2)$$

where  $S_{i,:}$  represents the cosine similarity for the  $i$ -th query.

#### 3.2. Local Stage

Global context features provide valuable semantic information that helps narrow down the candidate list. However, when faced with many semantically similar rooms, relying solely on global context is insufficient, and local features become increasingly essential. In this stage, we adopt a local perspective by first applying instance segmentation and the Receptive Field Expander to identify objects and patches. We then use the Object Feature Extractor to extract features from both objects and patches, followed by Object-Aware Scoring to further refine the candidate list.

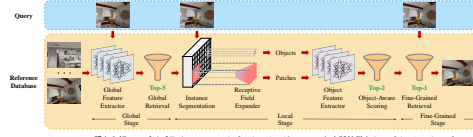


Figure 2. AirRoomの粗から細へのパイプライン. このパイプラインは、グローバルな文脈特徴をキャプチャしてトップ5の参照画像を検索するグローバル特徴抽出器から始まります。その後、インスタンスセグメンテーションが物体マスクを生成し、受容野拡張器が物体パッチを抽出します。物体特徴抽出器は、物体とパッチの特徴の両方を使用します。物体認識に最適化されたスコアリングモジュールが選択されたトップ2の候補に絞り、細かい検索が最も適切な参照画像を識別します。

習得ベースのモデルが特徴マップを抽出し、局所特徴を統合して包括的なグローバル記述子を生成するようになりました。しかし、ほとんどのVPRアプローチの高性能パフォーマンスは、VPR専用のデータセットでの大規模なトレーニングによるものです[18]。屋外のシーンのデータ収集は、屋外の天気、季節の変動が自然に存在するため比較的簡単です。しかし、室内の部屋でのデータ収集はより困難であり、屋内のデータセットでの大規模なトレーニングが難しく、その発展を制限する可能性があります。私たちのアプローチは、物体指向の特徴表現に焦点を当てることで、この課題を効果的に解決します。この設計により、AirRoomは特定のデータセットでの追加のトレーニングや微調整なしで強力なパフォーマンスを提供することができます。

### 3. 提案手法

我々は、図 Figure 2 に示すように、多段階の物体指向情報を活用した部屋認識のためのパイプラインでありながら非常に効果的なパイプライン、AirRoom を提案します。次に、パイプラインの各モジュールを、それらが実行される順序に従って体系的に紹介します。

#### 3.1. グローバル段階

この段階では、グローバル特徴抽出器を使用して、部屋内の物体の総合的な存在から得られるグローバルな文脈特徴をキャプチャします。これらの特徴は、グローバル検索に使用され、データベースからの類似した候補部屋を粗く選択するために使用されます。

##### 3.1.1. グローバル特徴抽出器

室内の部屋は、屋外環境と比べて変化が少ない。航空写真、水中といった多様な環境の特徴を欠き、昼夜や季節の変化といった時間的な変化も存在しない。そのため、大規模なデータセットでの大規模なトレーニングが難しく、その発展を制限する可能性があります。私たちのアプローチは、物体指向の特徴表現に焦点を当てることで、この課題を効果的に解決します。この設計により、AirRoomは特定のデータセットでの追加のトレーニングや微調整なしで強力なパフォーマンスを提供することができます。

しかしながら、屋内の部屋には本質的に多くの物体が存在し、それぞれが部屋全体の文脈の文脈に寄与している。このグローバルな文脈特徴を活用することで、参照検索をタスクと部屋と部屋に類似した部屋に絞って最適化することが可能となる。この目的のために、我々は大量の画像データセットで事前学習されたバックボーンを行って得ている。これらは高い汎用性を備え、多岐にわたるグローバルな文脈特徴を効果的に捉えることができるためである[17]。そのため、我々のモデル選択には、ResNet [14] のような CNN ベースの事前学習モデルや、DINOv2 [25] のようなトランスフォーマーベースの自己教師ありモデルが含まれる。

##### 3.1.2. グローバル検索

グローバル特徴抽出器を使用して、 $M$  個のクエリ画像と  $N$  個の参照画像に対してグローバルな文脈特徴を抽出します。クエリ特徴を  $Q \in \mathbb{R}^{M \times D}$ 、参照特徴を  $R \in \mathbb{R}^{N \times D}$  で表し、ここで  $D$  は特徴の次元を示します。コサイン類似度行列  $S$  は次のように計算されます:

$$S_{ij} = \frac{Q_i \cdot R_j}{\|Q_i\| \|R_j\|} \quad (1)$$

各クエリについて、次の式を使用して最も類似したトップ5の参照候補を選択します:

$$\text{Top}_5(S_{i,:}) = \text{arg-sort}(-S_{i,:})[:5]. \quad (2)$$

ここで、 $S_{i,:}$  は  $i$  番目のクエリに対するコサイン類似度行列を表します。

#### 3.2. ローカル段階

グローバルな文脈特徴は、候補リストを絞り込むために価値ある文脈情報を提供します。しかし、意図的に類似した部屋が多く存在する場合、グローバルな文脈だけに頼ることは不十分であり、局所特徴がますます重要になります。この段階では、最初にインスタンスセグメンテーションと受容野拡張器を使用して物体マスクとパッチを識別し、次に物体特徴抽出器を使用して物体とパッチの

(a) The first part of the English PDF of case 4.

(b) The first part of the Japanese PDF of case 4.

#### 3.2.1. Instance Segmentation

For each query image and its corresponding five candidates, we employ instance segmentation methods, such as Mask R-CNN [15] and Semantic-SAM [20], to identify and delineate individual objects. This process generates each object’s mask and bounding box. Next, we calculate the center point  $c$  of each object using its bounding box, as shown below:

$$c = \left( \frac{x + W}{2}, \frac{y + H}{2} \right) \quad (3)$$

In this equation,  $x$  and  $y$  represent the fixed coordinates of the top-left corner of the bounding box, while  $W$  and  $H$  denote the width and height of the bounding box, respectively.

#### 3.2.2. Receptive Field Expander

Single object information alone is not sufficiently discriminative. For example, although different desks may have distinct appearances, they can be found in both dining halls and offices. However, when an object is connected with its neighboring items—such as a desk alongside a computer, keyboard, or notebook—it suggests that the room is more likely to be an office rather than a dining hall. This insight motivates us to expand the receptive field from a single object to a patch containing multiple objects.

Given the center points of all objects in an image, we employ Delaunay triangulation [6] to generate a triangulated graph of object relationships. Specifically, Delaunay triangulation is applied to the set of object centers, ensuring that no object centers are inside the circumcircle of any triangle. This method maximizes the minimum angle of the triangles, preventing narrow, elongated triangles and ensuring more uniform object adjacency. By analyzing the adjacency relationships among the resulting triangles, we can construct the object adjacency matrix, which encodes the spatial and relational proximity of objects within the room.



Figure 3. The Receptive Field Expander broadens the receptive field from individual objects to patches rich in contextual information. Leveraging the object adjacency matrix and each object’s bounding box, it expands single objects such as a computer, window pane, and chair into object patches like a modular kitchen, multi-pane window, and dining set, respectively.

Given the object adjacency matrix and bounding boxes in an image, for each object, we consider the bounding boxes of its neighboring objects and enlarge the current object’s

bounding box to encompass all adjacent objects. This expansion processes the receptive field, enabling us to capture richer contextual information, as illustrated in Figure 3. We then apply Non-Maximum Suppression (NMS) to select the highest confidence bounding boxes, removing overlapping ones based on their Intersection over Union (IoU) scores. This results in a set of clean, informative object patches.

#### 3.2.3. Object-Aware Refinement

The Object-Aware Refinement module is composed of three key submodules: Object Feature Extractor, Mutual Nearest Neighbors, and Object-Aware Scoring.

**Object Feature Extractor** To effectively leverage object patches and object segmentation information, we prioritize global features over local feature aggregation. The latter approach may fail to capture object characteristics effectively and can significantly increase computational complexity and storage demands [49]. As discussed in Section 3.1.1, we continue to rely on models pre-trained on large image datasets. Using the Object Feature Extractor, we obtain features for both query and reference patches and objects. Let  $Q_o = \{q_i^o\}_{i=1}^5$  and  $Q_p = \{q_j^p\}_{j=1}^5$  represent the query patch and object feature sets, respectively. For each reference image among the query’s five candidates, we define the reference patch and object feature sets as  $R_p = \{r_i^p\}_{i=1}^5$  and  $R_o = \{r_j^o\}_{j=1}^5$ .

**Mutual Nearest Neighbors** Given a set of query features  $\{q_i^o\}_{i=1}^5$  and reference features  $\{r_j^o\}_{j=1}^5$ , we obtain feature pairs by identifying mutual nearest neighbor matches through exhaustive comparison of the two sets. Let  $P$  denote the set of cosine similarity scores for these mutual nearest neighbor matches, then we have

$$P = \{ \cos(q_i^o, r_j^o) \mid i \in \text{NN}_q(r_j^o), j \in \text{NN}_r(q_i^o) \} \quad (4)$$

where

$$\text{NN}_q(r_j^o) = \arg \max_i \left( \frac{q_i^o \cdot r_j^o}{\|q_i^o\| \|r_j^o\|} \right), \quad (5)$$

$$\text{NN}_r(q_i^o) = \arg \max_j \left( \frac{q_i^o \cdot r_j^o}{\|q_i^o\| \|r_j^o\|} \right), \quad (6)$$

$$\cos(q_i^o, r_j^o) = \frac{q_i^o \cdot r_j^o}{\|q_i^o\| \|r_j^o\|} \quad (7)$$

By utilizing mutual nearest neighbors, we can significantly improve retrieval accuracy, simultaneously narrowing the search space and enhancing overall retrieval efficiency [50].

**Object-Aware Scoring** The object-aware score is the sum of the global score  $s_{\text{global}}$  (calculated in Equation 1), the patch score  $s_{\text{patch}}$ , and the object score  $s_{\text{object}}$ :

$$s = s_{\text{global}} + s_{\text{patch}}(Q_p, R_p) + s_{\text{object}}(Q_o, R_o). \quad (8)$$

特徴を抽出します。その後、物体認識に最適化したスコアリングを行い、候補リストをさらに絞り込みます。

#### 3.2.1. インスタンスセグメンテーション

各クエリ画像とその対応する5つの候補について、Mask R-CNN [15] や Semantic-SAM [20] などのインスタンスセグメンテーション手法を用いて、個々の物体を識別し、輪郭を抽出します。このプロセスでは、各物体のマスクとバウンディングボックスが生成されます。次に、以下のようにして、各物体の中心点  $c$  をそのバウンディングボックスを用いて計算します:

$$c = \left( \frac{x + W}{2}, \frac{y + H}{2} \right) \quad (3)$$

この式では、 $x$  および  $y$  はバウンディングボックスの左上隅のピクセル座標を表し、 $W$  および  $H$  はそれぞれバウンディングボックスの幅と高さを示します。

#### 3.2.2. 受容野拡張器

単一の物体情報だけでは十分に識別的ではありません。例えば、異なるデスクは外見が異なるかもしれませんが、椅子やキーボード、ノートブックと一緒に見られることがあります。この洞察は、デスクがデスクの隣に椅子、キーボード、ノートブックがある場合—それはその部屋がオフィスではなくカフェである可能性が高いことを示唆します。この洞察は、受容野を単一の物体から複数の物体を含むパッチに拡張する動機となります。

部屋内のすべての物体の中心点が与えられた場合、Delaunay 三角分割 [6] を使用して物体間の関係の三角形グラフを生成します。具体的には、物体の中心点のセットに対して Delaunay 三角分割を適用し、任意の三角形の外縁の中に物体中心が含まれないことを確保します。この方法は三角形の最小角を最大化し、狭い細長い三角形を避ける。物体の隣接関係を分析することにより、部屋内の物体の空間的および関係的な近接性をエンコードする物体隣接行列を構築できます。



Figure 3. 受容野拡張器は、個々の物体から文脈情報に豊かなパッチの受容野の拡大を行います。図は、単一の物体（机）のバウンディングボックスを識別し、それを拡大して近隣の物体（コンピュータ、キーボード、ノートブック）を含めるように示しています。

物体隣接行列と画像内の物体のバウンディングボックスが与えられた場

合、各物体について、その隣接物体の境界ボックスを考慮し、現在の物体の境界ボックスを隣接するすべての物体を含むように拡大します。この拡張により受容野が増加し、より豊かな文脈情報を取得できるようになります。この拡張は図 3 に示す通り、その後、非最大抑制 (NMS) を適用して、最も高い信頼度の境界ボックスを選択し、その交差部分に基づいて重複するものを削除します。これにより、クリーンで情報豊富な物体パッチが得られます。

#### 3.2.3. 物体認識に最適化した改良

物体認識に最適化した改良モジュールは、物体特徴抽出器、相互最近傍、物体認識に最適化したスコアリングの3つの主要なサブモジュールで構成されています。

**物体特徴抽出器** 物体パッチと物体セグメンテーション情報を効果的に活用するために、局所特徴の集約よりもグローバル特徴を優先します。後者のアプローチは物体の特徴を効果的に捉えることができます。計算の複雑さやストレージの要求が大幅に増加する可能性があります[49]。セクション 3.1.1 で述べたように、大規模な画像データセットで事前学習されたモデル[15]に依存します。物体特徴抽出器を使用して、クエリと参照のパッチおよび物体の特徴を取得します。クエリのパッチと物体特徴セットをそれぞれ  $Q_p = \{q_i^p\}_{i=1}^5$  と  $Q_o = \{q_j^o\}_{j=1}^5$  とし、各参照画像について、参照のパッチと物体特徴セットを  $R_p = \{r_i^p\}_{i=1}^5$  と  $R_o = \{r_j^o\}_{j=1}^5$  と定義します。

**相互最近傍** クエリ特徴  $\{q_i^o\}_{i=1}^5$  と参照特徴  $\{r_j^o\}_{j=1}^5$  のセットが与えられた場合、両セットの徹底的な比較を通じて相互最近傍マッチを識別することにより、特徴ペアを取得します。P はこれらの相互最近傍マッチに対するコサイン類似度スコアのセットを示すことができ、次のようになります:

$$P = \{ \cos(q_i^o, r_j^o) \mid i \in \text{NN}_q(r_j^o), j \in \text{NN}_r(q_i^o) \} \quad (4)$$

ここで

$$\text{NN}_q(r_j^o) = \arg \max_i \left( \frac{q_i^o \cdot r_j^o}{\|q_i^o\| \|r_j^o\|} \right), \quad (5)$$

$$\text{NN}_r(q_i^o) = \arg \max_j \left( \frac{q_i^o \cdot r_j^o}{\|q_i^o\| \|r_j^o\|} \right), \quad (6)$$

$$\cos(q_i^o, r_j^o) = \frac{q_i^o \cdot r_j^o}{\|q_i^o\| \|r_j^o\|} \quad (7)$$

相互最近傍を利用することで、検索精度を大幅に向上させ、検索空間を縮小し、全体的な検索効率を高めることができます[50]。

**物体認識に最適化したスコアリング** 物体認識に最適化したスコア  $s$  は、グローバルスコア  $s_{\text{global}}$  (式 1 で計算)、

(c) The second part of the English PDF of case 4.

(d) The second part of the Japanese PDF of case 4.

Figure 9: Case 4 demonstrates the performance of LaTeXTrans on the En-Ja task



transformer [40] layers, denoted  $\{V_i\}_{i=1}^L$ . Given an input image  $x \in \mathbb{R}^{H \times W \times 3}$ , it is divided into  $M$  fixed-size patches, each projected into a patch embedding, resulting in  $E_0 \in \mathbb{R}^{M \times d_e}$ , where  $M$  represents the number of patches and  $d_e$  the embedding dimension. The initial patch embeddings  $E_0$  are combined with a learnable class token  $e_0$  and positional encodings, forming the input patch sequence for the transformer layers. Each layer processes this sequence as

$$[e_i, E_i] = V_i([e_{i-1}, E_{i-1}]) \quad i = 1, 2, \dots, L$$

After passing through all transformer layers, a patch projection layer,  $P_e$ , projects the output of the class token,  $e_L$ , into a shared V-L latent space,

$$f = P_e^*(e_L)$$

where  $f \in \mathbb{R}^d$ .  
**Text Encoding:** For an input text, e.g., "A photo of a [CLASS]", it is tokenized and converted into embeddings  $T_0 \in \mathbb{R}^{N \times d_t}$ , where  $N$  is the token length and  $d_t$  the embedding dimension. Beginning of text (EOT) and end-of-text (EOT) tokens, denoted  $b_0$  and  $e_0$ , mark the sequence boundaries. These token embeddings, with positional encodings, are passed through the text encoder  $W$ ,  $L$  transformer layers,  $\{W_i\}_{i=1}^L$ , as follows,

$$[b_i, T_i, e_i] = W_i([b_{i-1}, T_{i-1}, e_{i-1}]) \quad i = 1, \dots, L$$

After the final layer, the output of the EOT token,  $e_L$ , is projected into the shared V-L space using  $P_e$ ,

$$f = P_e(e_L)$$

where  $w \in \mathbb{R}^d$ .  
**Classification with CLIP:** With the image feature  $f$  and text features  $\{w_c\}_{c=1}^C$  for  $C$  classes, CLIP calculates the cosine similarity between  $f$  and each  $w_c$ ,

$$\text{sim}(f, w_c) = \frac{f \cdot w_c}{\|f\| \|w_c\|}$$

where  $\|\cdot\|$  represents the  $L_2$  norm. Class probabilities are then computed using the softmax function,

$$p(y = c | f) = \frac{\exp(\text{sim}(f, w_c)/\tau)}{\sum_{c=1}^C \exp(\text{sim}(f, w_c)/\tau)}$$

where  $\tau$  is a temperature parameter. The final predicted class is selected as the one with the highest probability score.

### 3.2. Multi-Modal Representation Learning (MMRL)

Our proposed MMRL aims to address the challenges of adapting pre-trained VLMs using few-shot data while maintaining generalization to new tasks. The training and inference frameworks of MMRL are shown in Fig. 2 and Fig. 3, respectively. In the following, we describe the specifics of the methodology.

#### 3.2.1. Learnable Representation Space

MMRL establishes a shared, learnable representation space  $\mathcal{R}$  to facilitate multimodal interactions, initialized through sampling from a Gaussian distribution. Using a learnable mapping function  $\mathcal{F}(\cdot)$ , implemented as a linear layer, we project the tokens  $R \in \mathbb{R}^{K \times d_r}$  in this space—where  $K$  is the number of tokens and  $d_r$  is the dimension of the representation space—into both visual and textual modalities,

$$R^v = \{\mathcal{F}(R_i^v)\}_{i=1}^K, \quad R^t = \mathcal{F}^*(R)$$

$$R^v = \{\mathcal{R}_i^v\}_{i=1}^K, \quad R^t = \{\mathcal{R}_i^t\}_{i=1}^K$$

where  $\mathcal{R}_i^v \in \mathbb{R}^{K \times d_e}$  and  $\mathcal{R}_i^t \in \mathbb{R}^{K \times d_t}$  represent the representation tokens for visual and textual modalities, respectively, in the  $(i+1)$ -th transformer layer. The index  $i$  indicates the starting layer from which these representation tokens are integrated into the encoder.

#### 3.2.2. Integration into Higher Encoder Layers

To preserve the generalized knowledge in the lower layers of the pre-trained CLIP model, the representation tokens  $R^v$  and  $R^t$  are integrated into the higher layers of the image encoder  $V$  and the text encoder  $W$ , beginning from the  $J$ -th layer.

For the image encoder  $V$ ,

$$[e_i, E_i] = V_i([e_{i-1}, E_{i-1}]) \quad i = 1, \dots, J-1$$

$$[e_i, E_i] = V_i([e_{i-1}, R_{i-1}^v, E_{i-1}]) \quad i = J, \dots, L-1$$

$$[e_i, R_i^v, E_i] = V_i([e_{i-1}, R_{i-1}^v, E_{i-1}]) \quad i = L$$

For the text encoder  $W$ , while previous prompt learning [17] involves replacing parts of  $T_i$  to incorporate deep prompts, we retain the entire  $T_i$  and insert  $R^t$  before it, aiming to preserve the original textual information.

$$[b_i, T_i, e_i] = W_i([b_{i-1}, T_{i-1}, e_{i-1}]) \quad i = 1, \dots, J-1$$

$$[b_i, T_i, e_i] = W_i([b_{i-1}, R_{i-1}^t, T_{i-1}, e_{i-1}]) \quad i = J, \dots, L-1$$

$$[b_i, R_i^t, T_i, e_i] = W_i([b_{i-1}, R_{i-1}^t, T_{i-1}, e_{i-1}]) \quad i = L$$

Note that due to the autoregressive nature of the text encoder, we adjust the attention mask matrix to accommodate the increased embedding length.

#### 3.2.3. Representation Learning

Representation learning is designed to leverage representation tokens for dataset-specific adaptation, while the class token preserves the pre-trained knowledge of the original CLIP. Through a set of strategies aimed at retaining generalization during both training and inference, MMRL enables flexible inference for different tasks, as detailed below.

- **Training Phase:** We optimize the features of both the representation tokens and the original class token, with

### 3. 方法

私たちのアプローチは、従来の手法に沿って、事前学習済みの VLM である CLIP [34] を基盤としています。このセクションでは、MMRL 画像フレームワークの構成と実装の詳細について説明します。

#### 3.1. 前提

私たちのアプローチで使用する記法を定義することから始めます。CLIP は、2 つのエンコーダーから構成されます: 画像エンコーダー  $V$  とテキストエンコーダー  $W$  です。

**画像エンコーディング:** 画像エンコーダーは、 $L$  層のトランスフォーマー [40] から構成され、これを  $\{V_i\}_{i=1}^L$  と表します。入力画像  $x \in \mathbb{R}^{H \times W \times 3}$  が与えられると、それは  $M$  個の固定サイズのパッチに分割され、それぞれがパッチ埋め込みに投影され、 $E_0 \in \mathbb{R}^{M \times d_e}$  が得られます。ここで、 $M$  はパッチの数、 $d_e$  は埋め込み次元を表します。最初のパッチ埋め込み  $E_0$  は、学習可能なクラストークン  $e_0$  および位置エンコーディングを組み合わせて、トランスフォーマー層への入力シーケンスが形成されます。各層はこのシーケンスを次のように処理します。

$$[e_i, E_i] = V_i([e_{i-1}, E_{i-1}]) \quad i = 1, 2, \dots, L$$

すべてのトランスフォーマー層を通した後、パッチ投影層  $P_e$  が、クラストークン  $e_L$  の出力を共有された V-L 潜在空間に投影します。

$$f = P_e^*(e_L)$$

ここで、 $f \in \mathbb{R}^d$  です。

**テキストエンコーディング:** 入力テキスト、例えば "A photo of a [CLASS]" の場合、それはトークン化され、埋め込み  $T_0 \in \mathbb{R}^{N \times d_t}$  に変換されます。ここで、 $N$  はトークン長、 $d_t$  は埋め込み次元を表します。テキストの開始トークン (EOT) および終了トークン (EOT) は、それぞれ  $b_0$  および  $e_0$  で示され、シーケンスの境界を示します。これらのトークン埋め込みは位置エンコーディングとともにテキストエンコーダーの  $L$  層のトランスフォーマー層  $\{W_i\}_{i=1}^L$  を通過します。次のように処理します。

$$[b_i, T_i, e_i] = W_i([b_{i-1}, T_{i-1}, e_{i-1}]) \quad i = 1, \dots, L$$

最終層後、EOT トークン  $e_L$  の出力は、 $P_e$  を使用して共有 V-L 空間に投影されます。

$$w = P_e(e_L)$$

ここで、 $w \in \mathbb{R}^d$  です。  
**CLIP による分類:** 画像特徴  $f$  と  $C$  クラスのテキスト特徴  $\{w_c\}_{c=1}^C$  を用いて、CLIP は  $f$  と各  $w_c$  のコサイン類似度を計算し、

$$\text{sim}(f, w_c) = \frac{f \cdot w_c}{\|f\| \|w_c\|}$$

ここで、 $\|\cdot\|$  は  $L_2$  ノルムを表します。クラス確率は次のソフトマックス関数を用いて計算されます。

$$p(y = c | f) = \frac{\exp(\text{sim}(f, w_c)/\tau)}{\sum_{c=1}^C \exp(\text{sim}(f, w_c)/\tau)}$$

ここで、 $\tau$  は温度パラメータです。最終的に予測されたクラスは、最も高い確率スコアを持つクラスとして選択されます。

### 3.2. Multi-Modal Representation Learning (MMRL)

我々が提案する MMRL は、少数ショットデータを使用し事前学習済みの VLM の応答に関する課題を解決し、同時に新しいタスクへの一般化を維持することを目的としています。MMRL の前提および推論フレームワークは、それぞれ Fig. 2 および Fig. 3 に示されています。以下に、方法論の詳細について説明します。

#### 3.2.1. 学習可能な表現空間

MMRL は、マルチモーダル相互作用を促進するために共有の学習可能な表現空間  $\mathcal{R}$  を確立します。この空間は、ガウス分布からサンプリングすることで初期化されます。学習可能なマッピング関数  $\mathcal{F}(\cdot)$  を使用し、これは線形層として実装され、トークン  $R \in \mathbb{R}^{K \times d_r}$  をこの空間に投影します。ここで  $K$  はトークンの数、 $d_r$  は表現空間の次元を表します。一般的およびテキストのモダリティに対して、

$$R^v = \{\mathcal{F}(R_i^v)\}_{i=1}^K, \quad R^t = \mathcal{F}^*(R)$$

$$R^v = \{\mathcal{R}_i^v\}_{i=1}^K, \quad R^t = \{\mathcal{R}_i^t\}_{i=1}^K$$

ここで  $\mathcal{R}_i^v \in \mathbb{R}^{K \times d_e}$  および  $\mathcal{R}_i^t \in \mathbb{R}^{K \times d_t}$  は、それぞれ視覚的およびテキストのモダリティにおける  $(i+1)$  層目での表現トークンを表します。インデックス  $i$  は、これらの表現トークンがエンコーダーに統合される開始層を示します。

**3.2.2. 高層エンコーダーへの統合**  
 事前学習済み CLIP モデルの下層における一般化された知識を保持するために、表現トークン  $R^v$  および  $R^t$  は、画像エンコーダー  $V$  およびテキストエンコーダー  $W$  の高層に統合され、 $J$  層目から始まります。

画像エンコーダーの場合、

$$[e_i, E_i] = V_i([e_{i-1}, E_{i-1}]) \quad i = 1, \dots, J-1$$

$$[e_i, E_i] = V_i([e_{i-1}, R_{i-1}^v, E_{i-1}]) \quad i = J, \dots, L-1$$

$$[e_i, R_i^v, E_i] = V_i([e_{i-1}, R_{i-1}^v, E_{i-1}]) \quad i = L$$

テキストエンコーダー  $W$  の場合、従来のプロンプト学習 [17] では  $T_i$  の一部を置き換え (deep プロンプト) を学習していますが、我々は  $T_i$  全体を保持し、その前に  $R^t$  を挿入することで、元のテキスト情報を保持するこ

(a) The first part of the English PDF of case 5.



Figure 3. MMRL inference process, where different tasks utilize distinct features.

the primary focus on representation features to preserve pre-trained knowledge. Specifically, the projection layer for the representation tokens is trainable, while that for the class token remains fixed. For the image encoder  $V$ , after passing through  $L$  transformer layers, we obtain the output  $e_L \in \mathbb{R}^d$  for the class token and  $E_L \in \mathbb{R}^{K \times d_e}$  for the  $K$  representation tokens. The final output of the representation tokens,  $r_L$ , is derived by averaging across the  $K$  tokens,

$$r_L = \text{Mean}(E_L)$$

where  $r_L \in \mathbb{R}^{d_e}$ . We then apply the patch projection layer to map the outputs of both the class and representation tokens into the common V-L latent space, yielding the class features  $f_c$  and representation features  $f_r$ ,

$$f_c = P_e^*(e_L) \quad f_r = P_e^*(E_L)$$

Here,  $P_e^*$  is the original, frozen patch projection layer of CLIP for class features, while  $P_e^*$  for representation features is trainable. For the text encoder  $W$ , following the sequential nature of text, we map the EOT token  $e_L$ —as in the original CLIP model—after processing through  $L$  transformer layers into the common V-L space, yielding the text features,

$$w = P_e(e_L)$$

With the image features  $f_c$ ,  $f_r$ , and the text classifiers  $\{w_c\}_{c=1}^C$  for  $C$  classes, we apply cross-entropy loss to separately optimize the class and representation features,

$$\mathcal{L}_{\text{cls}} = -\sum_c \log p(y = c | f_c)$$

$$\mathcal{L}_{\text{rep}} = -\sum_c \log p(y = c | f_r)$$

where  $\mathbb{1}_c = 1$  if the image  $x$  belongs to class  $c$ , and  $\mathbb{1}_c = 0$  otherwise. To further preserve the generalization of class features, we maximize the cosine similarity between  $(f_c, w)$  and the frozen CLIP features  $(f_0, w_0)$ , explicitly guiding the training trajectory,

$$\mathcal{L}_{\text{sim}} = 1 - \frac{f_c \cdot f_0}{\|f_c\| \|f_0\|}, \quad \mathcal{L}_{\text{sim}}^* = 1 - \frac{1}{C} \sum_c \frac{w_c^* \cdot w_0^*}{\|w_c^*\| \|w_0^*\|}$$

The final MMRL loss function is

$$\mathcal{L}_{\text{MMRL}} = \alpha \mathcal{L}_{\text{cls}} + (1 - \alpha) \mathcal{L}_{\text{rep}} + \lambda (\mathcal{L}_{\text{sim}} + \mathcal{L}_{\text{sim}}^*)$$

where  $\alpha$  controls the balance between the features, and  $\lambda$  is the penalty coefficient.

- **Testing on Base Classes:** For in-distribution classes seen during training, we combine the dataset-specific representation features with the class features that preserve generalizability. The probability of an in-distribution test sample  $x$  belonging to the  $c$ -th class is

$$p(y = c | x) = \alpha \cdot p(y = c | f_c) + (1 - \alpha) \cdot p(y = c | f_r)$$

where  $f_c$  and  $f_r$  are features extracted from the class token and representation tokens, respectively.

- **Testing on Novel Classes:** For classes unseen during training or for new datasets, we rely solely on the class tokens, which retain generalized knowledge.

$$p(y = c | x) = p(y = c | f_c)$$

### 4. Experiments

Details on implementation, datasets, and computational cost are provided in the Supplementary Materials.

#### 4.1. Tasks and Datasets

We conduct four core evaluations to comprehensively assess MMRL's performance: base-to-novel generalization, cross-dataset evaluation, domain generalization, and few-shot learning. Except for few-shot learning, all experiments utilize a 16-shot setting, i.e., only 16 training examples per category.

**Base-to-Novel Generalization:** In this evaluation, dataset classes are equally divided into base and novel classes. The model is trained exclusively on base classes and tested on both base and novel classes, allowing us to examine its transfer learning effectiveness on base classes as well as its ability to retain the inherent generalization or zero-shot capabilities of pre-trained VLMs for novel classes. We conduct this evaluation across 11 diverse image classification datasets: ImageNet [7], Caltech101 [9], OxfordPets [23], StanfordCars [19], Flowers102 [20], Food101 [13], FGV-Circraft [27], SUN397 [45], UCF101 [30], DTD [6], and EuroSAT [11].

とを目的とする。

$[b_i, T_i, e_i] = W_i([b_{i-1}, T_{i-1}, e_{i-1}]) \quad i = 1, \dots, J-1$   
 $[b_i, T_i, e_i] = W_i([b_{i-1}, R_{i-1}^t, T_{i-1}, e_{i-1}]) \quad i = J, \dots, L-1$   
 $[b_i, R_i^t, T_i, e_i] = W_i([b_{i-1}, R_{i-1}^t, T_{i-1}, e_{i-1}]) \quad i = L$

テキストエンコーダーの自己回帰的性質により、埋め込み表が複雑するため、注意マスク行列を調整していることに注意してください。

#### 3.2.3. 表現学習

表現学習は、表現トークンを活用してデータセットへの適応を行うことを目的としており、一方でクラストークンは元の CLIP が持つ事前学習済みの知識を保持します。学習および推論の両方において一般化を維持することを目的とした一連の戦略を通じて、MMRL はさまざまなタスクに柔軟な推論を可能にします。以下はその詳細を示します。

• **Training Phase:** 表現トークンおよび元のクラストークンの特徴を最適化し、事前学習済みの知識を保持するために主に表現特徴に焦点を当てます。具体的には、表現トークン用の投影層は学習可能であるのに対し、クラストークン用の投影層は固定されています。画像エンコーダー  $V$  において、 $L$  層のトランスフォーマー層を通した後、クラストークンの出力  $e_L \in \mathbb{R}^d$  と  $K$  個の表現トークンの出力  $E_L \in \mathbb{R}^{K \times d_e}$  を得る。表現トークンの最終出力  $r_L$  は、 $K$  個のトークンを平均化することで得られます。

$$r_L = \text{Mean}(E_L)$$

ここで、 $r_L \in \mathbb{R}^{d_e}$ 。次に、クラスおよび表現トークンの出力を共通の V-L 潜在空間にマッピングするためにパッチ投影層を用い、クラス特徴  $f_c$  および表現特徴  $f_r$  を得る。

$$f_c = P_e^*(e_L) \quad f_r = P_e^*(E_L)$$

ここで、 $P_e^*$  は CLIP のクラス特徴用の元の凍結されたパッチ投影層であり、 $P_e^*$  は表現特徴用の学習可能な層である。表現トークン  $R^t$  においては、テキストの逐次的性質に反し、元の CLIP モデルと同様に、 $L$  層の

とを目的とする。

$[b_i, T_i, e_i] = W_i([b_{i-1}, T_{i-1}, e_{i-1}]) \quad i = 1, \dots, J-1$   
 $[b_i, T_i, e_i] = W_i([b_{i-1}, R_{i-1}^t, T_{i-1}, e_{i-1}]) \quad i = J, \dots, L-1$   
 $[b_i, R_i^t, T_i, e_i] = W_i([b_{i-1}, R_{i-1}^t, T_{i-1}, e_{i-1}]) \quad i = L$

テキストエンコーダーの自己回帰的性質により、埋め込み表が複雑するため、注意マスク行列を調整していることに注意してください。

3.2.3. 表現学習  
 表現学習は、表現トークンを活用してデータセットへの適応を行うことを目的としており、一方でクラストークンは元の CLIP が持つ事前学習済みの知識を保持します。学習および推論の両方において一般化を維持することを目的とした一連の戦略を通じて、MMRL はさまざまなタスクに柔軟な推論を可能にします。以下はその詳細を示します。

• **Training Phase:** 表現トークンおよび元のクラストークンの特徴を最適化し、事前学習済みの知識を保持するために主に表現特徴に焦点を当てます。具体的には、表現トークン用の投影層は学習可能であるのに対し、クラストークン用の投影層は固定されています。画像エンコーダー  $V$  において、 $L$  層のトランスフォーマー層を通した後、クラストークンの出力  $e_L \in \mathbb{R}^d$  と  $K$  個の表現トークンの出力  $E_L \in \mathbb{R}^{K \times d_e}$  を得る。表現トークンの最終出力  $r_L$  は、 $K$  個のトークンを平均化することで得られます。

$$r_L = \text{Mean}(E_L)$$

ここで、 $r_L \in \mathbb{R}^{d_e}$ 。次に、クラスおよび表現トークンの出力を共通の V-L 潜在空間にマッピングするためにパッチ投影層を用い、クラス特徴  $f_c$  および表現特徴  $f_r$  を得る。

$$f_c = P_e^*(e_L) \quad f_r = P_e^*(E_L)$$

ここで、 $P_e^*$  は CLIP のクラス特徴用の元の凍結されたパッチ投影層であり、 $P_e^*$  は表現特徴用の学習可能な層である。表現トークン  $R^t$  においては、テキストの逐次的性質に反し、元の CLIP モデルと同様に、 $L$  層の

(c) The second part of the Chinese PDF of case 5.

(d) The second part of the Japanese PDF of case 5.

Figure 10: Case 5 demonstrates the performance of LaTeXTrans on the En-Ja task

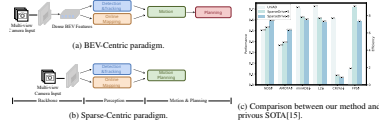


Figure 1: The comparison of various end-to-end paradigms. (a) The BEV-Centric paradigm. (b) The proposed Sparse-Centric paradigm. (c) Performance and efficiency comparison between (a) and (b).

motion prediction and planning should consider the high-order and bidirectional interactions among road agents. However, previous methods typically adopt a sequential design for motion prediction and planning, ignoring the impact of ego vehicle on surrounding agents. (2) Accurate prediction for future trajectories requires semantic information for scene understanding, and geometric information to predict future movement of agents, which is applicable to both motion prediction and planning. While these information are extracted in upstream perception tasks for surrounding agents, it is overlooked for ego vehicle. (3) Both motion prediction and planning are multi-modal problems with inherent uncertainty, but previous methods only predict deterministic trajectory for planning.

To this end, we propose SparseDrive, a Sparse-Centric paradigm as shown in Fig. 1b. Specifically, SparseDrive is composed of a symmetric sparse perception module and a parallel motion planner. With the decoupled instance feature and geometric anchor as complete representation of one instance (a dynamic road agent or a static map element), **Symmetric Sparse Perception** unifies detection, tracking and online mapping tasks with a symmetric model architecture, learning a fully sparse scene representation. In **Parallel Motion Planner**, a semantic-and-geometric-aware ego instance is first obtained from ego instance initialization module. With the ego instance and surrounding agent instances from sparse perception, motion prediction and planning are conducted simultaneously to get multi-modal trajectories for all road agents. To ensure the rationality and safety for planning, a hierarchical planning selection strategy that incorporating a collision-aware rescoring module is applied to select the final planning trajectory from multi-modal trajectory proposals.

With above effective design, SparseDrive unleashes the great potential of end-to-end autonomous driving, as shown in Fig. 1c. Without bells and whistles, our base model, SparseDrive-B, greatly reduces the average L2 error by 19.4% (0.58m vs. 0.72m) and collision rate by 71.4% (0.06% vs. 0.21%). Compared with previous SOTA (state-of-the-art) method UniAD[15], our small model, SparseDrive-S achieves superior performance among all tasks, while running 7.2× faster for training (20 h vs. 144 h) and 5.0× faster for inference (9.0 FPS vs. 1.8 FPS).

The main contribution of our work are summarized as follows:

- We explore the sparse scene representation for end-to-end autonomous driving and propose a Sparse-Centric paradigm named SparseDrive, which unifies multiple tasks with sparse instance representation.
- We revise the great similarity shared between motion prediction and planning, correspondingly leading to a parallel design for motion planner. We further propose a hierarchical planning selection strategy incorporating a collision-aware rescoring module to boost the planning performance.
- On the challenging nuScenes[1] benchmark, SparseDrive surpasses previous SOTA methods in terms of all metrics, especially the safety-critical metric collision rate, while keeping much higher training and inference efficiency.

2

(a) The first part of the English PDF of case 6.

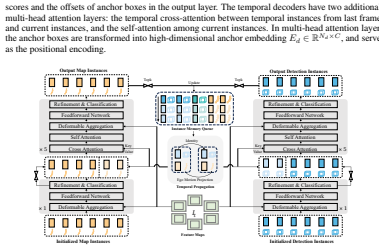


Figure 3: Model architecture of symmetric sparse perception, which unifies detection, tracking and online mapping in a symmetric structure.

**Sparse Online Mapping.** Online mapping branch shares the same model structure with detection branch except different instance definition. For static map element, the anchor is formulated as a polyline with  $N_p$  points:

$$\{x_0, y_0, x_1, y_1, \dots, x_{N_p-1}, y_{N_p-1}\}.$$

Then all the map elements can be represented by map instance features  $F_m \in \mathbb{R}^{N_m \times C}$  and anchor polylines  $L_m \in \mathbb{R}^{N_m \times N_p \times 2}$ , where  $N_m$  is the number of anchor polylines.

**Sparse Tracking.** For tracking, we follow the ID assignment process of SparseDrive[33]: once the confidence of an instance surpasses a threshold  $Th_{track}$ , it is locked onto a target and assigned with an ID, which remains unchanged throughout temporal propagation. This tracking strategy does not need any tracking constraints, resulting in an elegant and simple symmetric design for sparse perception module.

### 3.3 Parallel Motion Planner

As shown in Fig. 4, the parallel motion planner consists of three parts: ego instance initialization, spatial-temporal interactions and hierarchical planning selection.

**Ego Instance Initialization.** Similar to surrounding agents, ego vehicle is represented by ego instance feature  $F_e \in \mathbb{R}^{1 \times C}$  and ego anchor box  $B_e \in \mathbb{R}^{1 \times 1 \times 1}$ . While ego feature is typically randomly initialized in previous methods, we argue that the ego feature also requires rich semantic and geometric information for planning, similar to motion prediction. However, the instance features of surrounding agents are aggregated from image feature maps  $J$ , which is not feasible for ego vehicle, since ego vehicle is in blind area of cameras. Thus we use the smallest feature map of front camera to initialize the ego instance feature:

$$F_e = \text{AveragePool}(J_{fronts}) \quad (1)$$

There are two advantages in doing so: the smallest feature map has already encoded the semantic context of the driving scene, and the dense feature map serves as a complementary for motion

5

(c) The second part of the Chinese PDF of case 6.

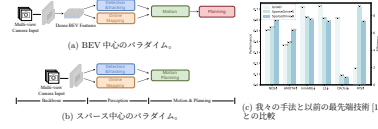


Figure 1:さまざまなエンドワンドのバライダイムの比較。(a) BEV 中心のバライダイム。(b) 提案されたスパース中心のバライダイム。(c) (a) と (b) の性能および効率の比較。

測することを目指して、モーション予測と計画は、道路エージェント間の高次および双方向的な相互作用を考慮する必要があります。しかし、従来の手法は通常、モーション予測と計画に対して順次的な設計を採用しており、自車両が周囲のエージェントに与える影響を無視しています。(2) 将来の軌道を正確に予測するためには、シーン理解のためのセマンティック情報と、エージェントの将来の動きを予測するための幾何学的情報が必要です。これらの情報は、周囲のエージェントに対する上流の短タスクで抽出されますが、自車両に対しては見過されされています。(3) モーション予測と計画は、いずれも不確実性を内包するマルチモーダルな問題ですが、従来の手法では計画に対して決定論的な軌道のみを予測しています。

これらに対して、我々は SparseDrive、スパース中心のバライダイムを提案します。図 1b に示すように、SparseDrive は対称的なスパース短尾ジュールと並列モーションプランナーで構成されています。インスタンス特徴と幾何学的アンカーを、一つのインスタンス（動的エージェントまたは静的マップ要素）の完全な表現として分離し、**対称的なスパース知覚**は、検出、追跡、オンラインマップとオンラインマップを統合的なアーキテクチャで統一し、完全なスパースシーン表現を学習します。**並列モーションプランナー**では、セマンティックおよび幾何学的に認識された自車両インスタンスが、最初に自車両インスタンス初期化モジュールから得られます。自車両インスタンスと周囲のエージェントインスタンスからスパース知覚から得られ、モーション予測と計画は同時に実行され、すべての道路エージェントに対してマルチモーダルな軌道が得られます。計画の合理性と安全性を確保するために、衝突認識型リスコアモジュールを組み込んだ階層的な計画選択戦略が適用され、マルチモーダルな軌道提案から最終的な計画軌道が選択されます。

これらの効果的な設計により、SparseDrive はエンドツーエンドの自動運転の大きな可能性を開きます。図 1c に示すように、設計な影響なしに、我々の基本モデルである SparseDrive-B は、平均 L2 誤差を 19.4% (0.58m vs. 0.72m) 減少させ、衝突率を 71.4% (0.06% vs. 0.21%) 削減しました。従来の SOTA（最先端技術）手法である UniAD[15] と比較して、我々の小型モデルである SparseDrive-S は、すべてのタスクで優れた性能を発揮し、トレーニングでは 7.2 倍、推論では 5.0 倍速く実行されます（トレーニング時間：20 時間 vs. 144 時間、推論速度：9.0 FPS vs. 1.8 FPS）。

我々の研究の主な貢献は以下の通りです：

- エンドツーエンドの自動運転におけるスパースなシーン表現を探索し、スパースなインスタンス表現を用いて複数のタスクを統一するスパース中心のバライダイムである SparseDrive を提案します。
- モーション予測と計画の間に存在する大きな類似性を修正し、それに対応する形でモーションプランナーの並列設計を提案します。さらに、計画性能を向上させるために、衝突認識型リスコアモジュールを組み込んだ階層的な計画選択戦略を提案します。
- 難易度の高い nuScenes[1] ベンチマークにおいて、SparseDrive は全ての指標で従来の最先端技術（SOTA）を上回り、特に安全性に関わる指標である衝突率において優れた結果を示し、さらにトレーニングおよび推論効率が大幅に向上しています。

2

(b) The first part of the Japanese PDF of case 6.

スパース検出ブランチは、 $N_{det}$  個のデコーダーで構成され、1つの非時間的デコーダーと  $N_{det}-1$  個の時間的デコーダーが含まれます。各デコーダーは、特徴マップ、インスタンス特徴  $F_i$  およびアンカーボックス  $B_i$  を入力として取り、更新されたインスタンス特徴と幾何学的アンカーボックスを出力します。非時間的デコーダーはラウドに初期化されたインスタンスを入力として受け取り、時間的デコーダーの入力は現在のフレームと過去のフレームの両方から来ます。具体的には、非時間的デコーダーは、変形可能な集約、フィードフォワードネットワーク（FFN）、および改変された分割のための注意力の3つのサブモジュールを含みます。変形可能な集約モジュールは、アンカーボックス  $B_i$  周辺に固定または学習可能なキーポイントを生じ、それらを特徴マップに投影して特徴をサンプリングします。インスタンス特徴  $F_i$  はサンプリングされた特徴と加算することによって更新されます。出力でアンカーボックスの分割スコアとオフセットを予測する役割を担います。時間的デコーダーには、2つの追加的なマルチヘッドアテンション層があります：前フレームと現在のインスタンス間の時間的クロスアテンション、および現在のインスタンス間の自己アテンション。マルチヘッドアテンション層では、アンカーボックスは高次元のアンカー埋め込み  $B_i \in \mathbb{R}^{N_{det} \times C}$  に変換され、位置エンコーディングとして機能します。

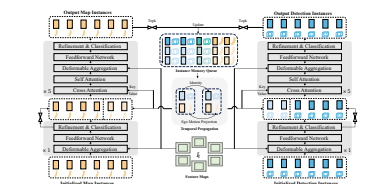


Figure 3: 対称的なスパース短尾のモデルアーキテクチャであり、検出、トラッキング、オンラインマップを対称的な構造で統一しています。

**スパースオンラインマップピング.** オンラインマップピングブランチは、検出ブランチと同じモデル構造を共有しますが、インスタンス定義が異なります。静的マップ要素の場合、アンカーは  $N_p$  点を持つラインとして定義されます。

$$\{x_0, y_0, x_1, y_1, \dots, x_{N_p-1}, y_{N_p-1}\}.$$

次に、すべてのマップ要素は、マップインスタンス特徴  $F_m \in \mathbb{R}^{N_m \times C}$  とアンカーポリライン  $L_m \in \mathbb{R}^{N_m \times N_p \times 2}$  によって表現されます。ここで、 $N_m$  はアンカーポリラインの数です。

**スパーストラッキング.** トラッキングについては、SparseDrive[33] の ID 割り当てプロセスに従いますが、インスタンスの検出信頼度が閾値  $Th_{track}$  を超えると、ターゲットにロックされ、ID が割り当てられ、時間的伝播を通じてその ID は変更されません。このトラッキング戦略は、トラッキング制約を必要とせず、スパース知覚はジェーブルのための後継でジェンルな対称的な設計を実現します。

### 3.3 並列モーションプランナー

図 4 に示すように、並列モーションプランナーは3つの部分で構成されています：自車両インスタンスの初期化、空間・時間的相互作用、および階層的な計画選択。

**自車両インスタンスの初期化.** 周囲のエージェントと同様に、自車両は自車両インスタンス特徴  $F_e \in \mathbb{R}^{1 \times C}$  と自車アンカーボックス  $B_e \in \mathbb{R}^{1 \times 1 \times 1}$  によって表現されます。自車特徴は以

5

(d) The second part of the Japanese PDF of case 6.

Figure 11: Case 6 demonstrates the performance of LaTeXTrans on the En-Ja task

### Prompt Template for LLM-score

You are a professional translation evaluator. Given an English source paragraph and its {tgt\_language} translation, evaluate the translation quality according to the following criteria:

Faithfulness: How accurately and completely does the translation convey the meaning of the source text?

Fluency: Is the translation natural, idiomatic, and grammatically correct in {tgt\_language}?

Terminology and Formatting Consistency: Are all technical terms translated correctly and consistently throughout the paragraph? Is the formatting—such as emphasis, symbols, references, and structural markers—preserved where applicable?

Contextual Coherence: Does the translation maintain logical flow, appropriate pronoun/reference usage, and contextual consistency across sentences within the paragraph?

Score each dimension from 0 to 10. Then, compute a final overall score (0 to 10), reflecting the overall translation quality, and round it to one decimal place.

Only return the final overall score as a number. Do not include explanations, sub-scores, or any additional content.

Figure 12: The LLM uses this prompt, which scores each pair's translation unit one by one.

### Prompt Template 1 for Translator

You are a professional academic translator specializing in LaTeX-based scientific writing. Your task is to translate long LaTeX texts (including section titles and content) from English to {tgt\_language}, while strictly maintaining the integrity of LaTeX syntax.

In addition to the LaTeX source, you are provided with:

1. A dynamic summary that condenses the content of all previous sections.
2. A bilingual term dictionary containing domain-specific English-{tgt\_language} term pairs.

You must use these resources to ensure translation quality:

- Use the summary to understand the document context, resolve ambiguous expressions, pronouns, or abstract references, and maintain coherence across sections.
- Strictly follow the term dictionary. If an English term in the source appears in the dictionary, you **must** use the corresponding {tgt\_language} translation from the dictionary without modification.

Please strictly follow the translation requirements below:

1. Only translate the natural language content while keeping all LaTeX commands, environments, references, mathematical expressions, and labels unchanged.
2. Section headings (e.g. natural content enclosed in {} in section identifiers like \section{}, \subsection{}, and \subsubsection{}) must also be translated, but their LaTeX syntax must remain unchanged.
3. Do not translate or modify the following LaTeX elements: Control commands: \label{}, \cite{}, \ref{}, \textbf{}, \emph{}, etc. Mathematical environments: \$...\$, [...], \begin{equation}...end{equation}, etc. Any parameter or argument that includes numerical values with LaTeX layout units such as: em, ex, in, pt, pc, cm, mm, dd, cc, nd, nc, bp, sp. Example: \vspace{-1.125cm} or [scale=0.58] → leave such expressions completely unchanged.
4. Do not change the writing of special characters, such as %, \#, \&, etc., to ensure that the translated text is accurate.
5. The final output must be a valid and compilable LaTeX document.
6. Ensure that the translated text is accurate, coherent, and follows academic writing conventions in the target language. Maintain consistent academic terminology and use standard abbreviations where appropriate.
7. Directly output only the translated LaTeX code without any additional explanations, formatting markers, or comments such as "latex".
8. <PLACEHOLDER\_CAP\_...>, <PLACEHOLDER\_ENV\_...>, <PLACEHOLDER\_...\_begin> and <PLACEHOLDER\_...\_end> are placeholders for artificial environments or captions. Please do not let them affect your translation and keep these placeholders after translation.

You are expected to combine semantic understanding (from the summary), precise terminology usage (from the term dictionary), and strict LaTeX fidelity to produce a high-quality translation.

Figure 13: Prompt template 1 for Translator, the Translator uses this prompt to initially translate the translation unit.

### Prompt Template 2 for Translator

You are a professional academic translator and LaTeX translation corrector. Your task is to revise and improve machine-translated LaTeX academic texts based on three components provided by the user: the original English LaTeX source ([Original]), the existing {tgt\_language} translation ([Translation]), and the error information describing the issue(s) ([Error Reports]). Your revision must strictly preserve LaTeX syntax integrity and comply with the following rules.

1. Only translate the natural language content while keeping all LaTeX commands, environments, references, mathematical expressions, and labels unchanged.
2. Section headings (e.g. natural content enclosed in {} in section identifiers like \section{}, \subsection{}, and \subsubsection{}) must also be translated, but their LaTeX syntax must remain unchanged.
3. Do not translate or modify the following LaTeX elements: Control commands: \label{}, \cite{}, \ref{}, \textbf{}, \emph{}, etc. Mathematical environments: \$...\$, [...], \begin{equation}...\end{equation}, etc. Any parameter or argument that includes numerical values with LaTeX layout units such as: em, ex, in, pt, pc, cm, mm, dd, cc, nd, nc, bp, sp. Example: \vspace{-1.125cm} or [scale=0.58] → leave such expressions completely unchanged.
4. Do not change the writing of special characters, such as \%, \#, \&, etc., to ensure that the translated text is accurate.
5. The final output must be a valid and compilable LaTeX document.
6. Ensure that the translated text is accurate, coherent, and follows academic writing conventions in the target language. Maintain consistent academic terminology and use standard abbreviations where appropriate.
7. Directly output only the translated LaTeX code without any additional explanations, formatting markers, or comments such as "latex".
8. <PLACEHOLDER\_CAP\_...>, <PLACEHOLDER\_ENV\_...>, <PLACEHOLDER\_...\_begin> and <PLACEHOLDER\_...\_end> are placeholders for artificial environments or captions. Please do not let them affect your translation and keep these placeholders after translation.

Only output the corrected LaTeX {tgt\_language} translation (revised version of '[Translation]'), with all changes implemented based on the '[Original]' and '[Error]'. Do not output the original input, explanations, or any extra content.

Figure 14: Prompt template 2 for Translator, the Translator uses this prompt and combines it with the error reports provided by the Validator to re-translate the translation unit.

### Prompt Template for Filter

You are a LaTeX translation assistant. Your task is to analyze the content inside any LaTeX environment, regardless of its environment name, and determine whether it should be translated when translating an academic paper.

Environment names can be custom-defined (e.g., 'mybox', 'resultblock', 'customalgo') and should be ignored during judgment. Only base your decision on the content itself.

Return 'True' if the content:

- Contains complete or partial sentences written in natural language (e.g., English), such as explanations, definitions, figure/table captions, theorem statements, or descriptions.
- Helps the reader understand the paper and would lose meaning if left untranslated.

Return 'False' if the content:

- Contains only code, pseudocode, mathematical formulas, drawing instructions (e.g., TikZ), formatting macros, or raw markup.
- Does not include any human-readable sentences or phrases.

Only output:

- 'True' or 'False'
- No explanations or additional text

Figure 15: Prompt template for Filter, the Filter uses this prompt to mark whether the translation unit needs to be translated.



### Prompt Template for Terminology Extractor

You are an en-`{tgt_language}` bilingual expert. Given an English source sentence and its corresponding `{tgt_language}` translation, your task is to extract all domain-specific terms from the English sentence, along with their exact translations as they appear in the `{tgt_language}` sentence.

These include:

- Technical terms and expressions
- Abbreviations or acronyms (e.g. RL, LM)
- Named entities or model names (e.g. COMET)
- Concept-specific noun phrases (e.g. optimization objective, long-term reward)

The translation must match exactly how it appears in the `{tgt_language}` sentence. Do not invent or guess new translations.

Output the result as a list of aligned term pairs in the following format:

"<English Term>" - "<`{tgt_language}` Translation>"

If there are no such terms, output: 'N/A'.

Figure 16: Prompt template for Terminology Extractor, Terminology Extractor uses this prompt to extract terms from each translation unit.

### Prompt Template for Summarizer

You are an academic summarization assistant designed to maintain an evolving semantic summary to support consistent and coherent machine translation of a long scientific document.

You will be given two inputs:

1. The current summary ('prev\_summary'), which reflects key information from all previously seen sections.
2. A new section of the document ('new\_section') that has not yet been summarized.

Your task is to:

- Integrate the new section's key content into the current summary, producing an updated summary.
  - Preserve previously summarized information that remains relevant.
  - Add any new findings, concepts, methods, or referential expressions introduced in the new section.
  - Ensure the summary remains concise, information-dense, and suitable for machine translation context support.
  - Do not repeat redundant content; merge semantically where possible.
- Use clear, academic English. The updated summary should be no more than 300 words.

Figure 17: Prompt template for Summarizer, the Summarizer uses this prompt to maintain the summary of the previous text.